Green Chemistry

TUTORIAL REVIEW

View Article Online
View Journal

Cite this: DOI: 10.1039/d1gc02307a

Polymeric carbon nitride-based photocatalysts for photoreforming of biomass derivatives

Jiu Wang, Pawan Kumar, Heng Zhao, Md Golam Kibria * and Jinguang Hu *

Photoreforming of biomass to value-added chemicals and fuels is a chemical approach to extract photosynthetically-trapped energy in complex biomolecules which otherwise disintegrate naturally in the environment. Designing precise photocatalytic materials that can selectively break the sturdy, nature-designed biomass with multiplex chemical composition/bonding and inaccessible sites is central to deploying this technology. Polymeric carbon nitride (CN) comprised of a 2D network of condensed heptazine/triazine (C_6N_7/C_3N_3) core has shown great promise for photoreforming of biomass derivatives due to intriguing physicochemical and optical properties. This review comprehensively summarizes the state-of-the-art applications of CN-based photocatalysts for the conversion of lignocellulosic biomass derivatives. Various chemical and structural modifications in CN structure such as doping, surface functionalization, hybridization entailing to higher selectivity and conversion have been discussed aiming at providing valuable guidance for future CN-based materials design.

Received 29th June 2021,
Accepted 16th August 2021

DOI: 10.1039/d1gc02307a

rsc.li/greenchem

1. Introduction

With the increasing carbon emissions and climate change, exploring a sustainable source of energy becomes an urgent task for the scientific community.[1,2] As the most available renewable resource, biomass has the potential to solve the increased energy demands through the environmentally-benign process, along with value-added chemicals.[3,4] It is estimated that global biomass is regenerated at a rate of about 100 billion tons per year.[5] The most abundant form of biomass, lignocellulose, has been regarded as a promising candidate for the production of fuels and chemicals.[6,7] Lignocellulosic

Department of Chemical and Petroleum Engineering, University of Calgary, 2500 University Drive, NW Calgary, Alberta, Canada. E-mail: md.kibria@ucalgary.ca, jinguang.hu@ucalgary.ca

Jiu Wang

Jiu Wang received his B.Sc. degree and M.Sc. degree from the Wuhan University of Technology with a major in Materials Science and Engineering in 2017 and 2020, respectively. He is currently pursuing his Ph.D. degree in Energy and Environment at the University of Calgary. His research work mainly focuses on the design and synthesis of functional catalysts for sustainable hydrogen and value-added products from sunlight-driven reforming of biomass.

Pawan Kumar

Dr Pawan Kumar obtained his Ph.D. in chemical science from the CSIR-Indian Institute of Petroleum, India in 2016. After his Ph.D., he worked as a post-doctoral fellow at Palacky University, Czech Republic and University of Alberta, Canada. Currently, he is working as a postdoctoral researcher at the University of Calgary, Canada. Dr Kumar is a recipient of the "Emerging Material Chemistry Investigator Award" from the Canadian Society for Chemistry. Dr Kumar's research interest is mainly focused on materials synthesis and their application in photocatalysis/photoelectrocatalysis (CO_2 reduction, water splitting, biomass photo-reforming to value-added chemicals, etc.*), catalysis (organic transformation), and energy applications.*

biomass is divided into cellulose, hemicellulose, and lignin.[8] Cellulose is the major component of lignocellulosic biomass, which is a linear crystalline polymer consisting of glucose units linked by β-1,4-glycosidic bonds. Hemicellulose cross-links the cellulose fibrils and is a typical polysaccharide, mainly comprised of C_5 and C_6 sugars. Lignin is the major non-carbohydrate component primarily cross-linked by phenylpropanols and presents an irregular amorphous framework. The cross-linking of these components makes the utilization of lignocellulosic biomass quite challenging because of the demand to disrupt the robust structure.[9,10] The structure of lignocellulosic biomass and its three primary components is shown in Fig. 1.

Multiple strategies have been applied for the conversion of lignocellulosic biomass as feedstock, including biological processes and thermochemical methods.[11,12] For biological processes, a physicochemical pretreatment step is firstly needed to open up biomass structure. For example, hot liquid water, steam explosion, and ammonia soaking pretreatment can afford hemicellulose solubilization and lignin degradation, which improves accessibility between cellulose and cellulases.[13] Additionally, chemical pretreatment with dilute acid at 120–210 °C achieves the removal of hemicellulose by hydrolyzing it into mono-sugars, while alkali chemicals such as NaOH or $Ca(OH)_2$ have been adopted to cleave the linkages of lignin–carbohydrate.[14,15] However, detrimental effects on the environment, reactor corrosion and their energy-intensive nature make such processes less attractive. Albeit, the following biological processes, such as enzymatic hydrolysis and fermentation, can afford a fair selectivity under ambient conditions, sluggish conversion rate, and the requirement of a specialized reactor to sustain enzyme/microbial activities, which make them inefficient while incurring the extra cost of pretreatment.[16] Some thermochemical methods such as pyrolysis, hydrogenation, and gasification are widely investigated to produce biocrude, C5–C6 chemicals such as hydroxymethylfurfural (HMF) and furfural, and syn-gas (CO + H_2 mixture), which can be transformed into high molecular liquid hydrocarbon by the Fisher–Tropsch process. Unfortunately, such reactions are energy-intensive and require harsh conditions like high temperature and pressure, which increases energy consumption.[17] Additionally, due to complex structural constitution and high oxygen content, such processes require catalysts which can promote deoxygenation, hydrodeoxygenation, hydrogenolysis, decarboxylation, and hydrogenation of biomass under extreme conditions to get value-added chemicals. However, under such conditions, coking, tar formation, deactivation/poisoning of catalysts, and phase transition are some common issues. Noble/non-noble metal nanoparticles/alloys supported on acidic/basic or bifunctional supports with mesoporous/nanochannel structures (zeolites such as ZSM-5, SBA-15, MCM-141, activated carbon, Al_2O_3, CeO_2),[18–22] transition metal carbides (Mo_2C, W_2C),[23,24] phosphides (Ni_2P),[25] intermetallic compounds ($Ni_3Sn_{(1-4)}$)[26] and fractional composition compounds (Rh-$Ce_{0.14}Zr_{0.81}Mg_{0.05}O_2$)[27] have been widely explored for biomass utilization. However, challenges associated with catalytic site deactivation and durability still persist.

In recent years, photocatalysis has been adopted for hydrogen production,[28] carbon dioxide (CO_2) reduction,[29] degradation of pollutants,[30] and bacteria disinfection.[31] Compared with conventional catalytic reactions, photocatalytic reactions take advantage of the inexhaustible solar energy and are performed under benign conditions.[32] More recently, photoreforming of biomass derivatives to value-added chemicals with sustainable H_2 coproduction enables photocatalysis to stand out among the aforementioned catalytic reactions.[33,34] For

Heng Zhao

Dr Heng Zhao received his Ph.D. degree from the Wuhan University of Technology and majored in Material Science and Engineering in 2019. He is currently a GRI CFREF funded post-doctoral researcher in the department of Chemical and Petroleum Engineering at University of Calgary under the guidance of Dr Jinguang Hu, Dr Md Kibria and Dr Stephen Larter. His research mainly focuses on the design and synthesis of functional catalysts for sustainable hydrogen and value-added bio-product co-production from biomass photoreforming.

Md Golam Kibria

Dr Md. Golam Kibria is an Assistant Professor in the Department of Chemical and Petroleum Engineering at the University of Calgary, Canada. He received MSc and Ph.D. degrees from McMaster and McGill University, respectively. He worked as a Banting Fellow at the University of Toronto. He is interested in artificial photosynthesis, nanomaterials, heterogeneous catalysis, system design, techno-economic and life-cycle analysis for renewable fuels and feedstocks, including electro-/photo-catalysis for CO_2 conversion and water splitting for sustainable energy and environment. Dr Kibria is a recipient of the Academic Gold Medal, the Tomlinson Doctoral fellowship from McGill University, and the Green Talents Award from German Federal Ministry.

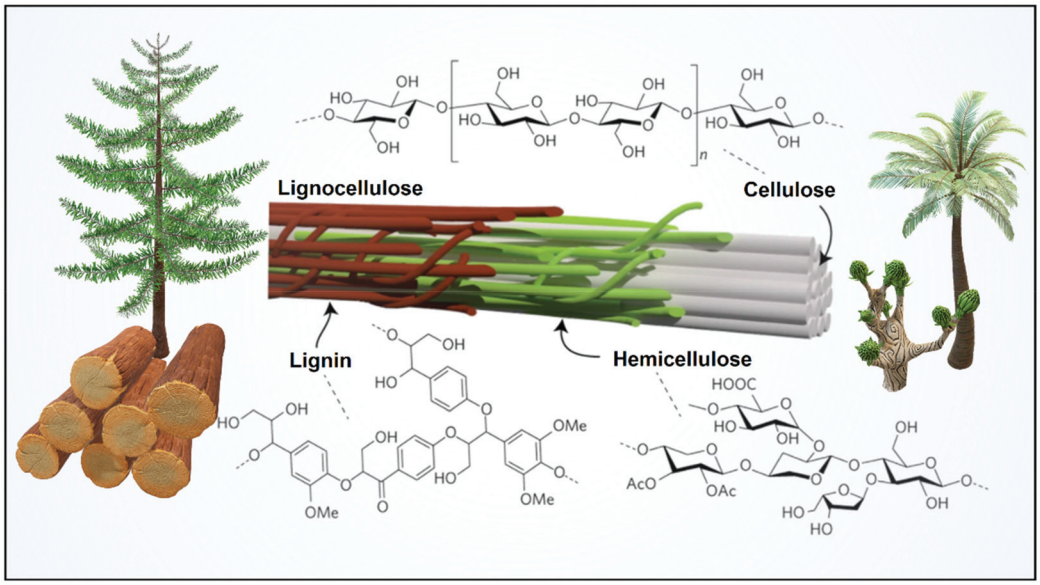

Fig. 1 The structure of lignocellulosic biomass and its primary components. Reproduced and modified from ref. 40 with permission from Springer Nature, copyright 2017.

efficient transfer of electrons/holes from the photocatalyst to the biomolecules, the HOMO and LUMO of molecules should be straddled by the leading energy edge (E_{CB} and E_{VB}) of the semiconductor. From the viewpoint of energetics, the biomass photoreforming is more thermodynamically favorable compared with energy-intensive water splitting due to the more positive oxidation potential (HOMO) of biomolecules.[35] However, biomass photoreforming still suffers from kinetically challenging reactions. The hydrogen-bonded crystalline cellulose amalgamated with lignin molecules makes bond-breaking sites inaccessible to the catalysts, leading to poor performance.[36]

To improve the accessibility of biomass to photocatalysts, pretreatment strategies such as acid/base treatment, enzymatic exfoliation and improved solubilization in ionic liquids [Bmim][$MeSO_4$] have also been combined with photocatalytic processes.[37,38] Apart from the kinetic factor of accessibility, biomass photoreforming also suffers from low solar utilization efficiency due to the intrinsic drawbacks of photocatalysts. As conventional photocatalytic materials, the role of titanium dioxide (TiO_2) and cadmium sulfide (CdS) in photocatalytic biomass reforming has been confirmed,[39–43] but the former is only active under ultraviolet irradiation and the latter is toxic and susceptible to photocorrosion. Other photocatalytic materials including homogeneous metal complexes (Ir, Ru polypyridyl complexes) and metal oxide/sulfide ($Znln_2S_4$, ln_2S_3, CuO_x/CeO_2) semiconductors operating in the visible regime have also been scrutinized for the biomass conversion.[6,7,10,11]

To decipher the other associated drawbacks of charge recombination, poor catalytic performance, and low resiliency, several strategies such as metal/heteroatom doping, surface area improvement, exposing specific active planes, nanostructure design, *etc.* have been thoroughly investigated.[44–48] Besides this, heterojunction formation is found to be the most promising due to the increased visible absorption, charge separation and improving stability. For example, heterojunctions formed by CdS with NiS,[49] P-doped $Zn_xCd_{1-x}S$,[50] $Ti_3C_2T_x$ [51] and $ZnIn_2S_4$,[52] and other heterojunctions such as TiO_2/NiO_x,[53,54] TiO_2/Bi_2WO_6,[55] and $Zn_{0.5}Cd_{0.5}S/MnO_2$ [56] have been successfully applied for the biomass valorization. Despite a favorable visible-light response, the performance of inorganic sulfide, oxides and mixed oxides/nitride-based photocatalysts remains too low for commercial implementation due to the

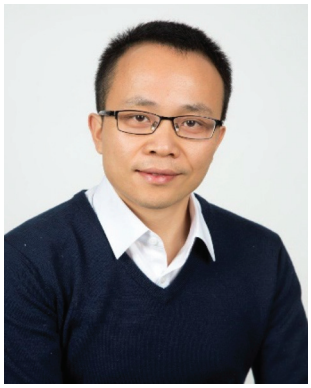

Jinguang Hu

Dr Jinguang Hu is an Assistant Professor in the Department of Chemical and Petroleum Engineering at the University of Calgary, Canada. He received Ph.D. degrees from the University of British Columbia, and did his postdoc at the UBC BioProducts Institute (Canada) and Aalto-VTT HYBER center (Finland), respectively. His current research is supported by the Canada First Research Excellence Fund (CFREF) and focuses on sustainable energy, biomass valorization, bioinspired materials/systems, and photo/bio-catalyst engineering for Energy and Environmental application. He is the External Advisory Board member of the Canada Biomass Energy Network and an active participator in the International Energy Agency (IEA) Bioenergy division.

short migration length of charge carriers in nanocrystals, photocorrosion, and inactivation/saturation of catalytic centers.[57]

The metal-free polymeric carbon nitride (C_3N_4; CN) constituting a 2D network of tertiary nitrogen-linked heptazine (C_6N_7) units has emerged as one of the most promising photocatalysts owing to low-cost preparation from Earth-abundant chemicals, strong physicochemical stability (~550 °C and stable in acid/base solution), unique electronic band structure (E_{CB}: −1.1 eV, E_{VB}: +1.6 eV) and a favorable visible-light response.[58,59] In this regard, CN can not only effectively utilize the visible light other than ultraviolet, but also maintain photocatalytic stability to avoid photocorrosion. The presence of primary (N–H) and secondary nitrogens (:NC_2) at the edge and a H-bonded uncondensed heptazine core provide plenty of catalytic centers to activate biomass substrate.[60,61] Indeed, CN has been utilized as metal-free catalysts for a variety of reactions (oxidation, epoxidation, esterification) including base-free reactions in mild conditions (three-component coupling).[62] The electron-rich 2D conjugated sheets also promote facile adsorption of biomass on CN sheets. On the one hand, CN with a less positive valence band cannot directly generate enough $^{\bullet}OH$ radicals thermodynamically, thus preventing over-oxidation/unselective oxidation of biomass derivatives.[58] Fortunately, a highly negative conduction band can compensate for the conversion rate as reductive electrons at the CB can reduce oxygen to generate $O_2^{\bullet-}$ radicals. The $O_2^{\bullet-}$ radicals would either participate directly in the reaction or produce secondary oxidants such as H_2O_2 and $^{\bullet}OH$ radicals.[63] Furthermore, the feasibility of band structure adjustment of CN by manipulating the chemical structure of carbon nitride through the incorporation of extraneous N-rich units, and changing the coordination pattern, provides an opportunity to rationally design more efficient and selective catalysts for biomass conversion.[64–66]

The present review traverses the recent development of the CN-based photocatalysts in the photoreforming of biomass derivatives. The fundamentals and the potential of the physicochemical properties of CN for biomass photoreforming have been discussed in detail. The review also summarizes the state-of-the-art applications of polymeric carbon nitride-based photocatalysts in the photoreforming of biomass derivatives, focusing on four main modification strategies: (1) hybrid heterostructures; (2) surface functionalization; (3) elemental doping and (4) other modifications. At the end of this review, we aim to provide critical comments on the opportunities of CN-based photocatalysts in biomass photoreforming and key challenges which may be encountered in the future.

2. Fundamentals of biomass photoreforming

As shown in Fig. 2, when the photocatalyst is exposed to a suitable light source with photon energy greater than the corresponding bandgap energy (E_g), the semiconductor photocatalyst generates charge carriers. In other words, the electrons (e^-) are promoted from the valence band (VB) to the conduction band (CB) leaving positive holes (h^+) in the valence band, resulting in photogenerated electron–hole pairs which initiate photoredox reactions. Not all the generated electrons and holes are translated to chemical energy as a significant fraction get recombined *via* non-radiative direct band to band, surface, and bulk recombination processes.[67,68] The electrons in the conduction band participate in the reduction process, the most common of which is the reduction of protons to form H_2. On the other hand, lignocellulosic biomass and its derivatives are oxidized by the holes on the valence band as sacrificial agents to obtain value-added products, thus reducing the

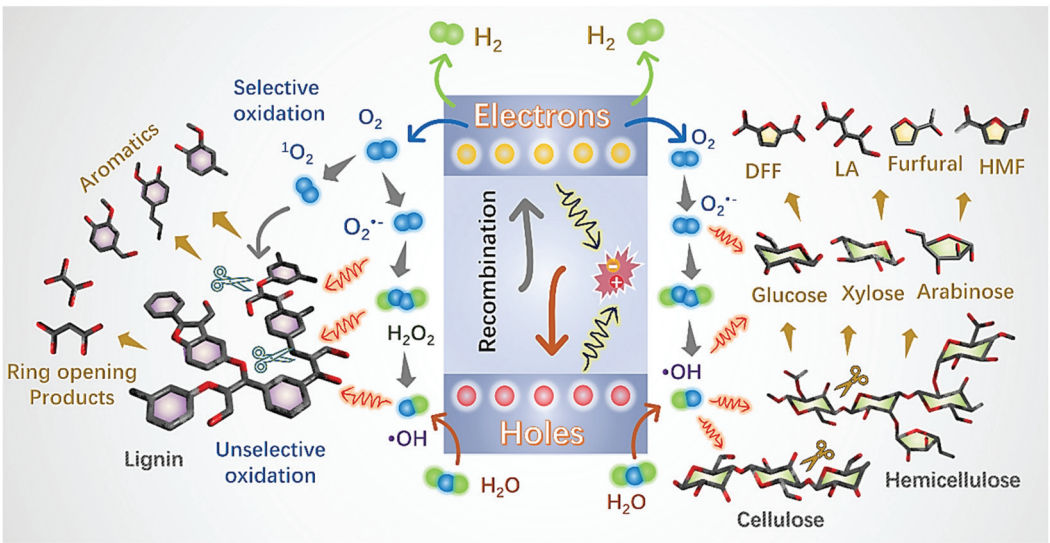

Fig. 2 The schematic illustration of photoreforming of biomass derivatives.

severe recombination rate of photogenerated electron–hole pairs.[69] Additionally, the organic molecules present in biomass contain plenty of oxygen-enriched functionalities (mainly –OH groups) with lone pairs of electrons in the non-bonding orbitals which can efficiently annihilate the photogenerated holes at the valence band leaving electron-deficient species.[70] These species can further donate protons at the conduction band under aprotic/neat conditions resulting in the co-generation of hydrogen and oxidized species.[71,72] However, under an aqueous environment, if catalysts possess oxidation potential more positive than water oxidation then protons generated from water oxidation predominantly participate in the hydrogen evolution step. Apart from that, another mechanism involves the reduction of oxygen at the CB and water oxidation at the VB. The reactions produce reactive oxygen species (ROS) such as oxygen anion radicals ($O_2^{\bullet-}$) and hydroxyl ($^{\bullet}OH$) radicals, which lead to the oxidation of biomass.[73] However, the biomass derivatives are prone to overoxidation to CO_2 rather than value-added chemicals. So, it is crucial to improve the selectivity of photooxidation products by limiting the overoxidation of biomass-derived intermediates. The oxidative holes can also generate hydroxyl radicals ($^{\bullet}OH$) by oxidizing water or hydroxyl ions (OH^-) which can promote biomass oxidation owing to their strong oxidizing power.[74,75] Furthermore, the biomass molecules can either be oxidized directly by holes or indirectly by ROS generated from electrons and holes such as $^{\bullet}OH$, $O_2^{\bullet-}$, and O_3^{-}.[10] Taking the degradation of lignin as an example, the existence of $^{\bullet}OH$ can effectively cleave β-O-4 linkages, leading to the production of low molecular weight chemicals such as catechol, resorcinol and hydroquinone. The chemical nature of ROS also has a significant influence on the mechanisms of biomass photooxidation.[76] Oxygen is easily reduced to superoxide anion radicals ($O_2^{\bullet-}$) if the photocatalytic process is exposed to air, potentially having an effect on the selectivity of the products. Hence, controlling the formation of ROS by altering the photocatalysts, reaction atmosphere, and solvent to obtain more desired chemicals from biomass derivatives is crucial.[70,77] The next sections will describe the unique physicochemical properties of polymeric carbon nitride (CN) and the potential of CN-based photocatalysts to be applied in biomass photoreforming.

3. Physicochemical properties of polymeric carbon nitride and its potential for biomass photoreforming

Recently, 2D carbonaceous materials have been widely investigated for biomass transformation due to their excellent electronic mobility, high surface area, formation of hybrid structure with other materials and synergistically enhanced activity. For example, the research group of Varma *et al.* has revisited the potential of 2D graphene derivatives and their heterostructure for transesterification reactions to produce biodiesel.[78] Another 2D semiconductor, polymeric carbon nitride (CN), displayed many advantages compared with other traditional inorganic semiconductor materials, *i.e.* moderate bandgap (2.7 eV with E_{CB}: −1.1 eV and E_{VB}: +1.6 eV *vs.* normal hydrogen electrode, NHE), which makes it suitable as a visible photocatalyst in biomass photoreforming.[79,80] Furthermore, due to the constrained oxidation ability of CN valence band holes, the population of generated hydroxyl radicals ($^{\bullet}OH$) remains low after being excited by visible light, which helps to achieve high selectivity of certain biomass conversion reactions.[63] Moreover, due to the strong van der Waals and H-bonding between layers, CN shows better chemical stability in various organic solvents, acid or alkali solvents, which have been adopted to improve biomass accessibility.[58] Since the formation rate and reactivity of radicals are highly dependent on the solvent and pH value,[81,82] CN can photocatalyze certain biomass conversion reactions in a wide range of reaction conditions. In addition, CN has C–N heterocycles with an aromatic-like structure, which makes it thermally stable in the air or inert atmosphere at 600 °C.[59] It can be easily prepared by low-priced nitrogen-rich precursors including melamine, urea, thiourea, and dicyandiamide. More importantly, CN contains only carbon and nitrogen, both of which are Earth-abundant elements. This implies the properties can be improved by simple strategies without an obvious alteration of its overall composition.[83] Furthermore, the polymeric nature makes it possible to achieve molecular-level modulation and surface functionalization.[58,59] For example, the tri-*s*-triazine (heptazine) structure of CN can serve as a support matrix to combine with other semiconductors,[84] metal nanoparticles,[85] and quantum dots.[86] This excellent compatibility is instrumental in the fabrication of polymeric carbon nitride-based photocatalysts for the photoreforming of biomass derivatives. Surface functionalization mainly involves grafting different functional groups in the plane structure of CN such as cyano (–C≡N) groups[87] and ethyl alcohol groups[88] for biomass photoreforming. Moreover, the periodic structure of CN contains abundant amino groups that can form hydrogen bonds, which provides favorable conditions for the incorporation of surface functional groups.[89] If surface functional groups are adequately modified, the hydrophilicity or hydrophobicity of CN could be tuned to better interact with biomass, thus giving rise to higher biomass conversion efficiency. Additionally, the sp^2-hybridized N atoms with lone-pair electrons can serve as Lewis basic sites,[90] potentially anchoring certain groups of the biomass substrate molecules. However, there are still several obstacles and shortcomings, such as severe photocharge carrier recombination, low conductivity and few surface-active sites, hindering its practical applications. Bulk CN suffers from severe charge carrier recombination due to the presence of inter/intra-sheets of hydrogen bonding between NH/NH_2 strands of uncondensed units working as charge trap centers.[91,92] Furthermore, the leading absorption of CN is limited to 450 nm (blue light) and only a tiny fraction of light is absorbed up to 550 nm, which reduces the quantum efficiency. To overcome these issues, various strategies such as elemental (metal/non-metal) doping, morphology modulation,

and construction of heterojunctions with various semiconductors have been developed to improve photocatalytic efficiency.[93–96] Modification methods, including nanostructure design, heterostructure construction, cocatalyst loading and electronic structure modulation, have been successfully demonstrated in overall water splitting,[97,98] photocatalytic hydrogen production,[99,100] CO_2 photoreduction,[101,102] and, more recently, for biomass photoreforming.[103,104] Furthermore, breaking the intersheet hydrogen bonding by the transformation of bulk CN to monolayer sheets can prevent localized charge recombination, exposing more active sites for the biomass transformation. The schematic diagram of polymeric carbon nitride-based (CN-based) photocatalysts for the photoreforming of biomass derivatives is shown in Fig. 3. The modification strategies for the application of CN-based photocatalysts in the photoreforming of biomass derivatives will be discussed in detail in the next section.

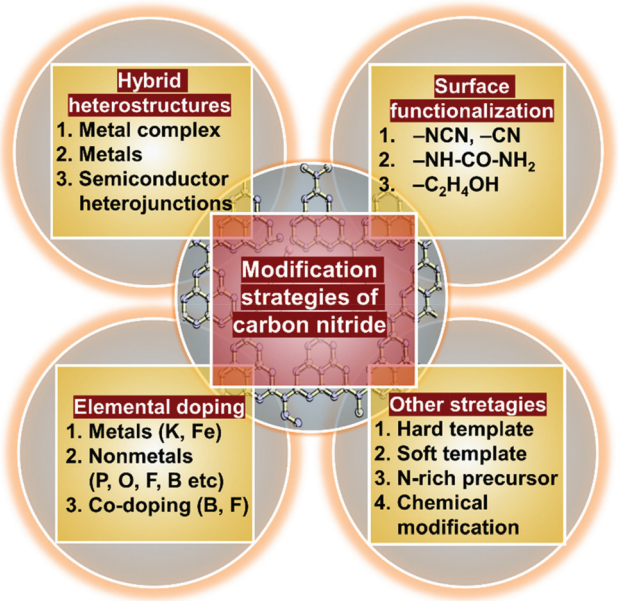

Fig. 4 Modification strategies of CN-based photocatalysts for biomass photoreforming.

4. Modified carbon nitride-based photocatalysts for biomass photoreforming

Acknowledging the potential of CN-based materials for biomass photoreforming, researchers are developing various modification methods to further enhance the photocatalytic activity of carbon nitride. In the following sections, the four key strategies for modification of CN-based photocatalysts for biomass photoreforming are discussed (Fig. 4), including hybrid heterostructures, surface functionalization, elemental doping and other modifications such as acid treatment, thermal exfoliation, solvent modulation, *etc*. The comprehensive summary of reported CN-based photocatalysts for the photoreforming of biomass derivatives is shown in Tables 1–4.

4.1 Hybrid heterostructures

The construction of hybrid heterostructures is an effective approach to improve the photocatalytic performance of the

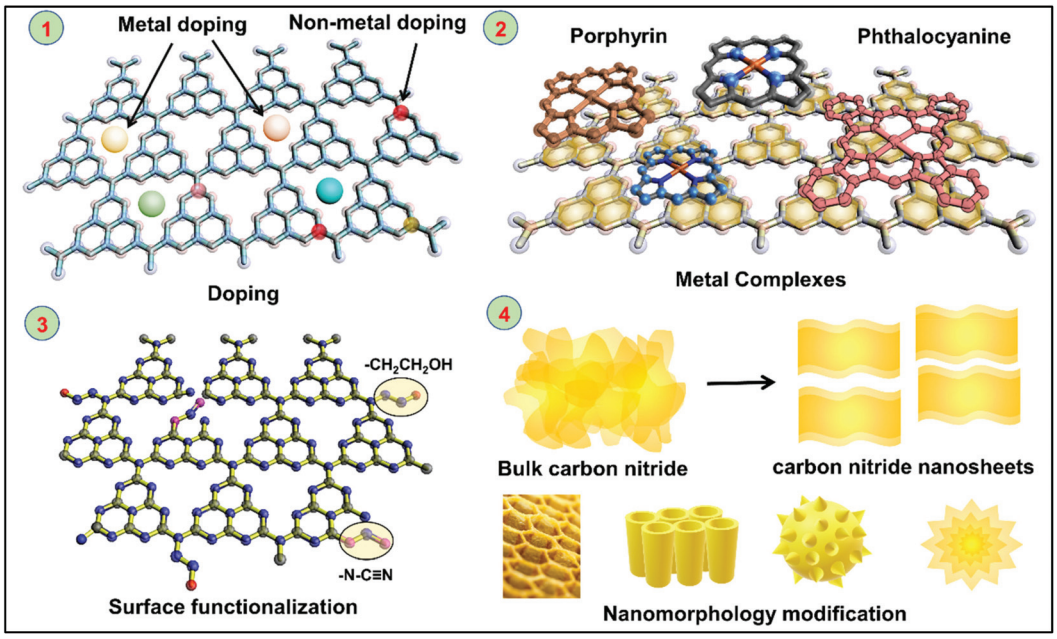

Fig. 3 Modification of CN-based photocatalysts for photoreforming of biomass derivatives. Hybrid heterostructure with (1) metals and non-metals, (2) metal complexes (3) surface group functionalization (4) nano-morphological modification such as sheets formation, surface area improvement and heterojunctions formation.

Table 1 The summary of CN-based photocatalysts for photoreforming of biomass derivatives by hybrid heterostructures

Photocatalyst	Substrate	Light source	Media	Main products (yield%)	Ref.
CoPz/g-C_3N_4	HMF	Xe lamp (500 mW cm^{-2})	$Na_2B_4O_7$ buffer solution	FDCA (96.1%)	113
CoPz/g-C_3N_4	Glucose	Xe lamp (300 W)	Water/30% aqueous H_2O_2 solution	Gluconic and glucaric acid (41.4%)	117
ZnPp-C_3N_4-TE	HMF	Natural solar light	Water	FDC (26.3%)	120
AgPd@g-C_3N_4	Vanillin	Visible light (40 W)	HCOOH	2-Methoxy-4-methylphenol (99%)	85
Pd/g-C_3N_4	Furfural	Xe lamp (λ > 420 nm)	CH_3CN/HCOOH/triethylamine	Furfuryl alcohol (27%)	128
Pt/g-C_3N_4	HMF	Xe lamp (λ > 420 nm)	Water/triethylamine	DHMF (4.5%)	129
WO_3/g-C_3N_4	HMF	Xe lamp (λ > 400 nm)	CH_3CN/$PhCF_3$	DFF (23.9%)	136
ZnS/g-C_3N_4	Glucose	Xe lamp (300 W)	Water	H_2 (209.4 μmol g^{-1})	137
CoO/g-C_3N_4	Cellulose	Xe lamp (300 W)	1 M NaOH	H_2 (178 μmol h^{-1} g^{-1})	84
$NaNbO_3$/g-C_3N_4	HMF	Xe lamp (λ > 400 nm)	Water	FFCA (31.3%)	138
QDs/g-C_3N_4	Furfural	Xe lamp (λ > 420 nm)	TEOA/NADH	Furfuryl alcohol (0.6 mM)	86
CN_x-Ni_2P	Cellulose	Simulated sunlight (100 mW cm^{-2})	0.5 M KOH	H_2 (38 μmol m^{-2} g^{-1})	139
MXene/g-C_3N_4	HMF	Xe lamp (λ > 400 nm)	Trifluorotoluene	DFF (90%)	140
$DMASnBr_3$/ g-C_3N_4	Glucose	Simulated solar light (500 W m^{-2})	Water	H_2 (925 μmol g^{-1} h^{-1})	146

Table 2 The summary of CN-based photocatalysts for photoreforming of biomass derivatives by surface functionalization

Photocatalyst	Substrate	Light source	Media	Main products (yield%)	Ref.
$^{NCN}CN_x$-NiP	Cellulose	Simulated sunlight (100 mW cm^{-2})	Phosphate solution	H_2 (1690 μmol h^{-1} g^{-1})	103
AKCN	Glucose	Visible light (λ > 420 nm)	Phosphate buffer solution	Gluconic acid	153
UCN-NA	Xylose	White LED light (5 W)	5 M NaOH	H_2 (136.9 μmol)	88
HCN-NEA	Xylose	Xe lamp (λ > 420 nm)	5 M NaOH	H_2 (122.77 μmol h^{-1})	154
PCN-H_2O_2	HMF	Natural solar light	Water	FDC (17.6%)	155

Table 3 The summary of CN-based photocatalysts for photoreforming of biomass derivatives by elemental doping

Photocatalyst	Substrate	Light source	Media	Main products (yield%)	Ref.
B@mCN-Y	Arabinose	Visible light irradiation	2 M KOH solution	Lactic acid (92.7%)	83
Ut-OCN	Xylose	Visible light irradiation	3 M KOH	Lactic acid (89.7%)	104
P@CN-SO_3H	Xylose	Visible light irradiation	0.1 M KOH	Xylonic acid (88.1%)	181

Table 4 The summary of CN-based photocatalysts for photoreforming of biomass derivatives by other modifications

Photocatalyst	Modification strategy	Substrate	Light source	Media	Main products (yield%)	Ref.
mpg-C_3N_4	Hard-template method	2-Phenoxy-1-phenylethanol	LED light (455 nm, 6 W)	CH_3CN	Benzaldehyde (51%)	188
SGCN	Hard-template method	HMF	LED light (100 mW cm^{-2}, λ > 400 nm)	Water	DFF (38.4%), H_2 (36 μmol m^{-2} h^{-1})	189
M-CNU	Hard-template method	THFA	390 nm LED	CH_3CN	GBL (64%)	190
g-C_3N_4	Soft-template method	HMF	Xe lamp (300 W, λ > 400 nm)	Water	DFF (26.7%)	193
MCN_520	Thermal exfoliation	HMF	Real outdoor illumination	Water	FDC (20%)	194
TE-520	Thermal exfoliation	HMF	Natural solar light	Water	FDC (26.3%)	195
o-g-C_3N_4	Acid treatment	Glucose	Natural solar light	Sea water	H_2 (2523 μmol h^{-1} g^{-1})	196
$^{NCN}CN_x$	Solvent modulation	Glucose	Simulated sunlight (100 mW cm^{-2})	25 wt% LiBr/0.1 M H_2SO_4/0.1 M LiOH	Arabinose (74.5 μmol h^{-1} g^{-1}), H_2 (112.8 μmol h^{-1} g^{-1})	197

photocatalysts by reducing the recombination of photogenerated electrons and holes. Numerous hybrid heterostructures of carbon nitride with metal complexes, metal nanoparticles, and semiconductors have been found to ameliorate the biomass conversion efficiency, which will be discussed in the following sections.

4.1.1 Metal complexes/carbon nitride heterostructures. Metal complexes such as phthalocyanines, porphyrins and polyazine are excellent photocatalysts due to their wide absorption (low HOMO–LUMO gap), product selectivity, high binding affinity for O_2 to generate an excited singlet oxygen ($^1O_2$) and unprecedented selectivity for the desired products.[105,106] Indeed, metal complexes can mimic the enzymatic catalysis due to the presence of single-site metal centers leading to highly selective conversion.[107] Unfortunately, the homogeneous nature of metal complexes makes them hard to recover incurring overall costs unsuitable for industrial applications. As 80% of the industrial catalysts are heterogeneous, hybridization of homogeneous metal complexes is a viable approach to make them recyclable while synergistically improving the photocatalytic performance. Carbon nitride is an ideal supporting material for the immobilization of metal complexes due to the presence of plenty of electron-rich nitrogen functionalities and a conjugated sp^2 C–N network facilitating the stabilization of metal complexes *via* π–π interaction.[108,109] The hybrid heterostructure strongly influences the electron acceptance and donation dynamics due to the alteration of the HOMO–LUMO position of metal complexes and carbon nitride, thus giving rise to strong interaction. Additionally, the aggregation of certain molecules which co-exist in dimeric to polymeric form (for example J and H aggregates) would be reduced by hybridization as well and, accordingly, achieve good dispersion. The combination of metal complexes and carbon nitride plays a significant role in enhancing photocatalytic activities, including extending light-absorption, serving as a trapping center for photogenerated carriers to achieve highly efficient charge separation and acting as a catalytic center for specific surface reactions.[110–112] For example, Xu *et al.* reported the synthesis of a biomimetic photocatalyst by combining cobalt thioporphyrazine (CoPz) and g-C_3N_4 coupled together with π–π interactions.[113] The developed catalysts displayed selective oxidation of 5-hydroxymethylfurfural (HMF) to 2,5-furandicarboxylic acid (FDCA) under simulated sunlight using oxygen as a benign oxidant. Interestingly, after hybridization of CoPz on g-C_3N_4, the intensity of absorption bands at shorter (B band) and longer (Q band) wavelengths was increased owing to reduced agglomeration, validating the strong action between CoPz and g-C_3N_4 (Fig. 5a). The Co_2p binding energy of CoPz/g-C_3N_4 was slightly decreased compared with CoPz after immobilization, suggesting the CoPz bind to g-C_3N_4 *via* axial coordination of Co_2^+ with N atoms (Fig. 5b). The characteristic XRD peak of g-C_3N_4 at ~27.5° was significantly weakened after the introduction of amorphous CoPz, revealing that good dispersion of CoPz was achieved on

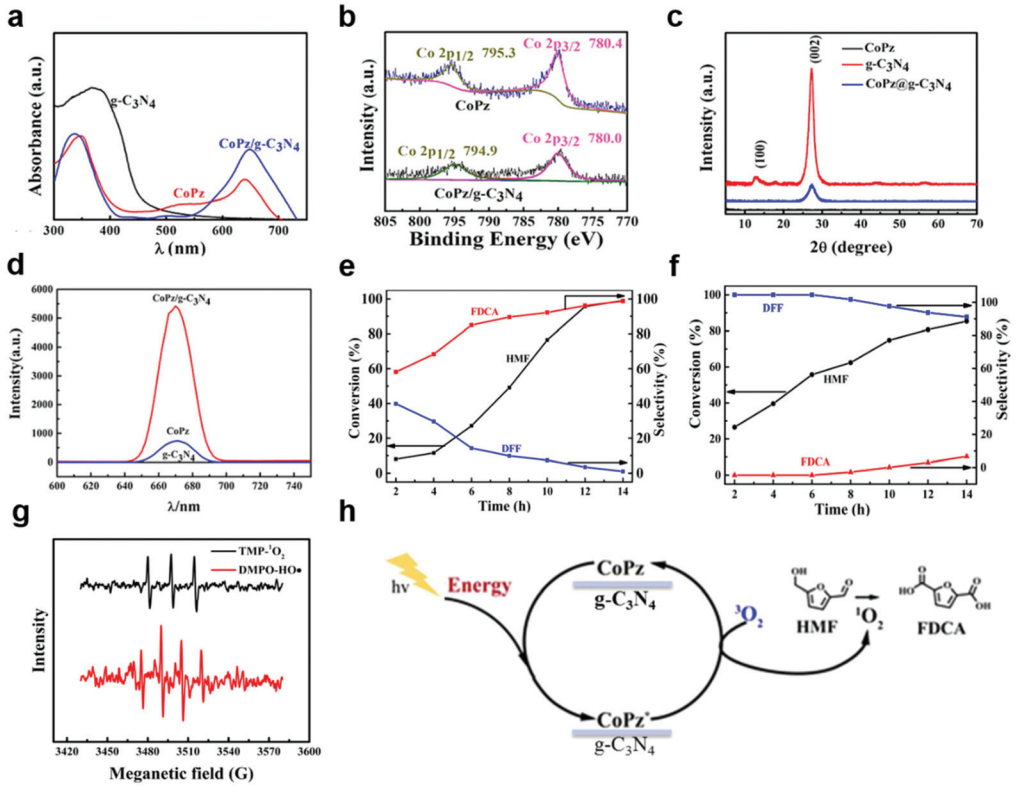

Fig. 5 (a) UV-Vis DR spectra, (b) Co_2p XPS spectra, (c) XRD patterns, (d) phosphorescence emission spectra of CoPz, g-C_3N_4, and CoPz/g-C_3N_4. Influence of pH of the reaction mixture on the photocatalytic performance: (e) pH-9.18, (f) pH-4.01. (g) EPR signals of the DMPO-HO$^\bullet$ adduct in water in the presence of bulk g-C_3N_4 and the TMP-$^1O_2$ adduct in water in the presence of CoPz/g-C_3N_4 in the photocatalysis process. (h) Possible mechanism of the photocatalytic oxidation of HMF into FDCA with the CoPz/g-C_3N_4 catalyst. Reproduced from ref. 113 with permission from ACS Publications, copyright 2017.

the surface of g-C_3N_4 (Fig. 5c). As shown in Fig. 5d, the phosphorescent intensity of CoPz/g-C_3N_4 was nearly six times that of CoPz at 670 nm, implying the stable electron interaction between CoPz and g-C_3N_4, owing to the empty d-orbital of Co_2^+ with free electrons or lone-pair electrons of g-C_3N_4. At pH-9.18 and under ambient temperature and pressure, an FDCA yield of 96.1% with a 99.1% conversion of HMF was achieved in aqueous media (Fig. 5e). When pH was decreased to 4.01, 2,5-diformylfuran (DFF) was observed as the main product (Fig. 5f). To investigate the role of the reactive species involved in the selective oxidation, dimethylpyridine *N*-oxide (DMPO) and 4-chloro-2-nitrophenol were used as $^{\bullet}OH$ radical and singlet oxygen ($^1O_2$) scavengers, respectively, which demonstrate that g-C_3N_4 produces unselective $^{\bullet}OH$ oxidants while CoPz/g-C_3N_4 produces singlet $^1O_2$ leading to unprecedented selectivity for HMF to FDCA. Electron paramagnetic resonance (EPR) spin-trapping was adopted to further verify the intrinsic mechanism. As shown in Fig. 5g, CoPz/g-C_3N_4 displayed an obvious signal of $^1O_2$, while the characteristic signal of $^{\bullet}OH$ was observed on g-C_3N_4. A possible mechanism for the photocatalytic oxidation of HMF into FDCA was proposed in Fig. 5h. In the CoPz/g-C_3N_4 photocatalyst, the presence of g-C_3N_4 increases the electronic density on Co_2^+ empty d orbitals by donating their π electrons, so Co_2^+ centers are activated easily to convert $^3O_2$ into $^1O_2$ under light irradiation achieving high selectivity of FDCA. Actually, HMF is an important platform chemical and FDCA has a high market value.[114] The photocatalytic processes under mild reaction conditions to convert HMF into FDCA is more environment-friendly than the other thermochemical or biological approaches. For example, noble metal catalysts such as Pt, Au, or Ru have usually been adopted to realize traditional thermochemical oxidation of HMF with harsh reaction conditions (high concentration of base and high temperature above 100 °C).[115] Additionally, a chloroperoxidase has been discovered to achieve HMF bio-oxidation, but this process is uneconomical owing to low FDCA yield (60–75%), higher yield of byproducts and high cost of the enzyme.[116] In another similar study, Zhang *et al.* synthesized a g-C_3N_4/CoPz composite by a facile mixing method to effectively produce gluconic acid and glucaric acid from glucose using H_2O_2 as an oxidant using a 300 W Xe lamp.[117] It was found that CoPz modification can enhance the accessibility between glucose and g-C_3N_4 and suppress the formation of nonselective $^{\bullet}OH$, preventing the over oxidation to afford high selectivity of gluconic and glucaric acid from glucose. Moreover, the g-C_3N_4/CoPz composite exhibits an enhanced visible light response and carrier separation efficiency, thus achieving 79.4% of total selectivity to gluconic and glucaric acid with 52.1% of glucose conversion. Taking glucose to gluconic acid as an example of a target reaction for comparison, thermochemical approaches can only realize this reaction using the metal-salt solution or noble-metal catalyst at ~110 °C, which is more energy-consuming than photocatalysis.[118,119] Porphyrin modified carbon nitride as heterogeneous photocatalysts for photooxidation of 5-hydroxymethylfurfural (HMF) to 2,5-furandicarboxaldehyde (FDC) under natural solar light was also reported.[120] The modified carbon nitride promoted light absorption and higher order in the porphyrin ring, thus leading to better performance of FDC selectivity. Among the as-prepared photocatalysts, the g-C_3N_4 supported by porphyrins containing a Zn(II) complex (ZnPp-C_3N_4-TE) exhibited the best performance at neutral pH, with a 73% HMF conversion and 36% FDC selectivity.

4.1.2 Metal nanoparticles/carbon nitride heterostructures. Metal nanoparticles have been adopted to construct hybrid heterostructures as they have catalytic sites which can cleave specific bonds and stabilize the intermediate state to get desired products.[121,122] Metal nanoparticles improve the charge separation efficiency as their low Fermi level works as an electron sink to capture photogenerated electrons.[123] Additionally, metal particles also increase activity and the visible light absorption due to surface plasmon resonance (SPR) in plasmonic metals such as Cu, Ag, Au.[124,125] When hybridized with semiconductor materials, the generated hot electrons on the metal can also couple with excitons (plasmon–exciton coupling) to activate high energy-demanding molecules.[126,127] Carbon nitride decorated with various metal nanoparticles has been demonstrated for diverse applications including biomass conversion. For examples, Verma *et al.* reported a bimetallic AgPd@g-C_3N_4 as an active photocatalyst for upgradation of biofuel *via* hydrogenation of vanillin, a lignin-derived molecule, under visible irradiation.[85] The surface area of AgPd@g-C_3N_4 was found to be 105 $m^2\ g^{-1}$, which was 3 times that of the pure g-C_3N_4 (35 $m^2\ g^{-1}$). The high surface area demonstrates that the incorporation of metal particles has favorable effects on the pore structure, thus improving the overall accessibility to active sites, along with achieving better dispersibility. Due to synergistic interactions of bimetallic centers with g-C_3N_4 support, the AgPd@g-C_3N_4 photocatalyst had achieved an astonishing 99% selectivity and almost 100% conversion of vanillin within 4 h at room temperature. Additionally, recycling experiments had shown that the AgPd@g-C_3N_4 catalyst was stable up to 10 cycles and afforded complete conversion of vanillin into 2-methoxy-4-methylphenol. Dong *et al.* reported a Pd-supported carbon nitride photocatalyst (Pd/g-C_3N_4) for hydrogenation from furfural to furfuryl alcohol with a yield of 27% under visible light.[128] Surface plasmon resonance (SPR) effect induced by Pd nanoparticles was found to facilitate the photoreduction process on Pd/g-C_3N_4. A Pt-supported carbon nitride catalyst (Pt/g-C_3N_4) was reported to realize photocatalytic reduction of 5-hydroxymethylfurfural (HMF) to 2,5-dihydroxymethylfuran (DHMF) under visible light as well.[129]

4.1.3 Semiconductors/carbon nitride heterojunctions. The hybridization of two semiconductors with an appropriate band structure called a heterojunction is advantageous as they can overcome the issue of limited visible absorption, charge separation, active sites and band potential requirements altogether.[130,131] Among various reported heterojunctions, type-II, Z-scheme, and S-scheme heterojunctions are most important.[132–134] In type-II or direct scheme heterojunctions, two semiconductors with small band position differences

combine together to give a staggered configuration in which electrons/holes travel from CB/VB on one semiconductor to another semiconductor. The Z-scheme which proceeds through the transfer of electrons from the CB of one semiconductor to the VB of the second semiconductor *via* two-photon excitation is more appealing as they can meet the demands of wide band positions while using two small band gap semiconductors.[135] Carbon nitride, due to its 2D nature and its ability to form heterojunctions with almost any semiconductor, has been widely investigated for biomass conversion. As the VB of the carbon nitride is less positive, the formation of the Z-scheme heterojunction with semiconductors possessing more oxidative VB can further ameliorate performance. For example, Zhang *et al.* proposed a WO_3/g-C_3N_4 composite by a direct calcination method for selective photocatalytic oxidation of 5-hydroxymethylfurfural (HMF) to 2,5-diformylfuran (DFF) under visible-light irradiation.[136] It was found that the incorporation of WO_3 into g-C_3N_4 triggers the Z-scheme mechanism, thus increasing the charge separation and facilitating the oxidation ability to convert HMF to DFF. The trapping studies using 1,4-benzoquinone (BQ), *tert*-butyl alcohol (*t*-BuOH), and ethylenediaminetetraacetic acid disodium salt (EDTA-Na_2) as $O_2^{\bullet-}$, $^{\bullet}OH$ and hole (h^+) scavengers indicated that $O_2^{\bullet-}$ and h^+ are the main active species to transform HMF to DFF. Xu *et al.* coupled the reforming of glucose with the photocatalytic hydrogen generation using a ZnS/g-C_3N_4 catalyst using a 300 W Xe lamp.[137] Redshift, better light absorption and reduced charge carrier recombination were achieved after the coupling of ZnS with g-C_3N_4, thus enhancing the hydrogen generation during the photoreforming process. Wu *et al.* developed a low-cost CoO/g-C_3N_4 catalyst for the coproduction of lactic acid and H_2 under visible-light irradiation.[84] Different synthetic methods including hydrothermal, photodeposition and one-pot calcination were attempted, among which the one-pot calcination has been demonstrated to afford the highest hydrogen evolution during cellulose photocatalytic degradation, which was adopted for further applications. The XPS results identified the existence of Co species (Co_2^+), Co–N and Co–O–C bonds (Fig. 6a). The strong interaction between CoO and g-C_3N_4 was further confirmed by K-edge X-ray absorption near-edge structure (XANES) (Fig. 6b). After the hybridization with g-C_3N_4, the absorption of Co K-edge shifts toward higher energy revealing the formation of Co–N bonding. As shown in Fig. 6c, the photoreforming of glucose produces lactic acid with an excellent ~78 wt% carbon preservation compared with the carbon content in glucose with concomitant H_2 co-production. Acid- and alkali-treated cellulose was also used as a substrate to evaluate the photoreforming performance (Fig. 6d). It was found that the highest activity was achieved by using phosphoric acid swollen cellulose (PASC) with more than 71 wt% conversion of cellulose after 12 h coupled with a hydrogen evolution rate of ~178 μmol h^{-1} g_{cat}^{-1}, attributed to the strong interaction between photocatalyst and biomass. Then, the different biomass pretreatment strategies were also investigated (Fig. 6e), which exhibited much higher hydrogen generation, cellulose conversions and lactic acid production compared with raw biomass. Specifically, the hydrogen generation production of the phosphoric acid pretreated wheat straw (PAPWS) was 15 times that of raw biomass (Fig. 6f). Zhu *et al.* synthesized a $NaNbO_3$/g-C_3N_4 composite for selective photocatalytic oxidation of 5-hydroxymethylfurfural (HMF) to 5-formyl-2-furancarboxylic acid (FFCA) under visible-light illumination.[138] The photocatalyst showed restrained charge recombination and $^{\bullet}OH$ production, and $O_2^{\bullet-}$ was regarded as the main active species during the oxidation process based on the trapping experiments. Yu *et al.* reported a CdSe/ZnS quantum dots (QDs) modified g-C_3N_4 catalyst for photobiocatalytic conversion of furfural (FAL) to furfuryl alcohol (FOL) under visible-light using alcohol dehydrogenase (ADH) and nicotinamide adenine dinucleotide (NADH) as an electron shuttle to direct the selectivity.[86] It was found that the QDs were dispersed uniformly on the surface of QD/g-C_3N_4 nanosheets, and the optimal QD loading was 5 wt%. The synergistic effects of ADH and regeneration of NADH leads to nearly 100% FOL selectivity. Additionally, the catalytic activity still remained over 70% after nine recycling experiments, which proved the high stability and reusability of the photocatalysts. A noble-metal-free (CN_x/Ni_2P) photocatalyst was reported for cellulose photoreforming to H_2 under simulated sunlight as well.[139]

Wang *et al.* reported a 2D/2D MXene/g-C_3N_4 composite for selective photocatalytic oxidation of HMF to DFF (2,5-diformylfuran) with a 97% selectivity and 90% yield of DFF within 10 h under visible-light irradiation.[140] Apart from photovoltaics, recently, halide perovskite (general formula ABX_3), either in the bulk thin film or as quantum dots due to unique small tunable band gaps (depending upon the halogen composition) and short better carrier mobility, has been explored for various photocatalytic applications including CO_2 reduction, hydrogen generation and organic transformation.[141,142] Unfortunately, the instability of halide perovskite in ambient air and moisture and toxic lead forbids their application in photocatalysis. Ligand exchange, a protective coating with thin oxide layers and graphene/graphene oxide have demonstrated promising stability; however, absorption and charge transfer to the substrate is compromised.[143,144] Carbon nitride, due to its semiconducting nature, visible absorption and formation of heterojunctions, is an appropriate choice for protection.[145] Recently, Speltini and coworkers demonstrated that dimethylammonium and phenylethylammonium-based perovskites—$DMASnBr_3$ and PEA_2SnBr_4— coupled with g-C_3N_4 can utilize glucose as a sacrificial donor for the hydrogen evolution reaction. Under solar simulated irradiation and using glucose as a hole scavenger the optimum HER was found to be 925 μmol g^{-1} h^{-1}, which was 15-fold higher than the performance of materials in pure water. Interestingly, the catalysis can also photoreform starch remaining active even after 3 recycling runs.[146]

In summary, most of the current studies on CN-based photocatalysts for the photoreforming of biomass derivatives are focused on hybrid heterostructures, as listed in Table 1.

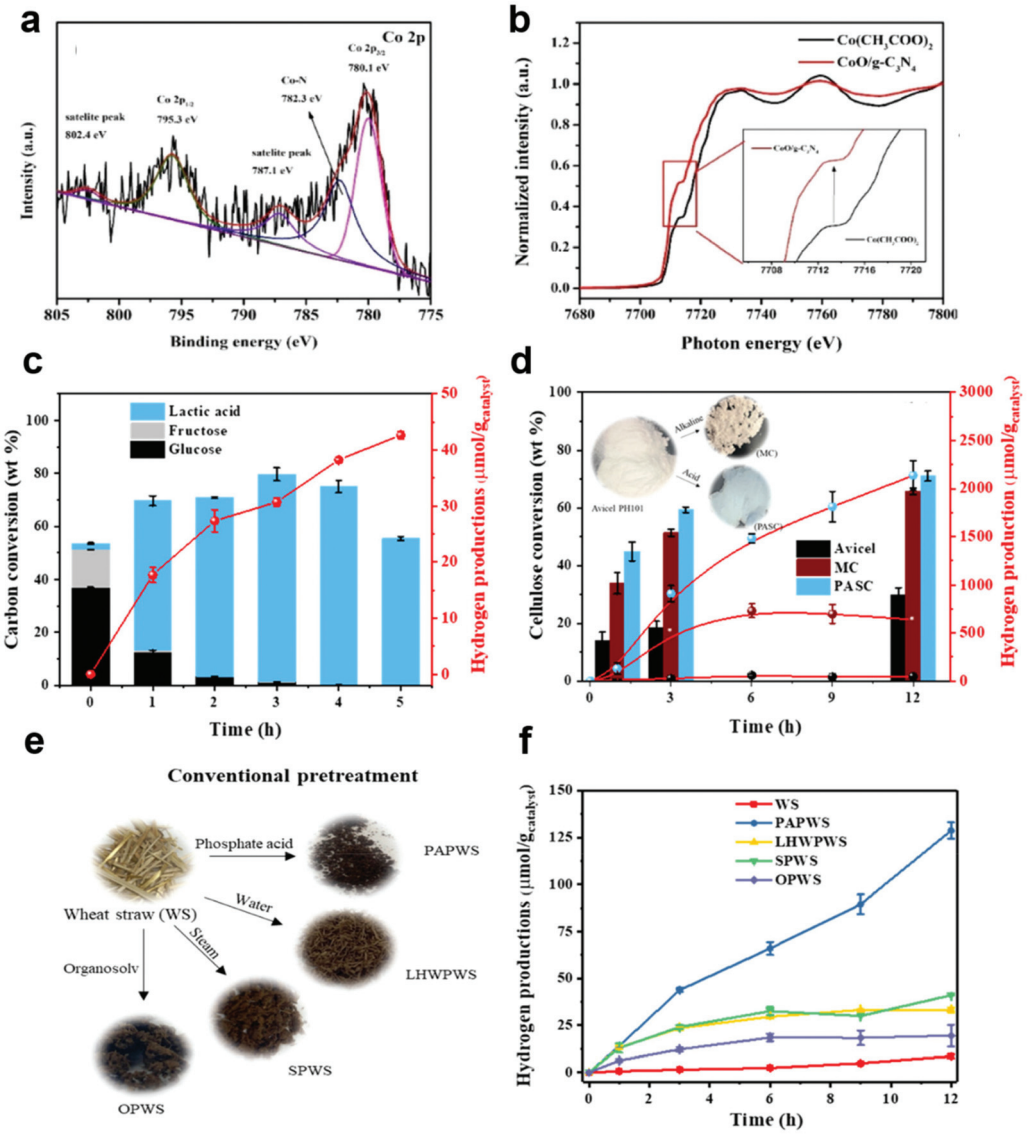

Fig. 6 (a) XPS spectra of CoO/g-C_3N_4 showing the Co_2p peak. (b) *Ex situ* XANES Co K-edge of CoO/g-C_3N_4 and cobalt acetate for comparison. (c) Glucose PR: carbon conversion of its product distribution and hydrogen production from 5 mg of glucose in 1 M NaOH solution using 10 mg of CoO/g-C_3N_4 under a 300 W Xe lamp. (d) Cellulose PR: cellulose conversion, hydrogen production from 5 mg of different modes of cellulose. (e) Images of raw and conventional pretreated WS. (f) Hydrogen production. Reaction conditions: 1 wt% cellulose, catalyst: CoO/g-C_3N_4 (10 mg), medium: 1 M NaOH, and light source (300 W Xe lamp), 12 h. Reproduced from ref. 84 with permission from ACS Publications, copyright 2020.

The CN is actually an ideal material to form hybrid heterostructures with metal complexes, metal nanoparticles and semiconductors due to its unique π-conjugated structure and desirable band position. Therefore, highly efficient charge separation and more active sites can be achieved for biomass photoreforming. All these hybrid heterostructures have successfully demonstrated the potential of CN to be applied in biomass photoreforming. However, most of the studies adopt model platform compounds such as glucose or HMF instead of native biomass, mainly due to the complex and sturdy structure. It is anticipated that the above-discussed works on the rational design of hybrid heterostructures of CN-based photocatalysts will direct research to achieve higher biomass conversion/selectivity and can be further applied to native biomass photoreforming.

4.2 Surface functionalization

The efficient interaction of organic biomass on the surface of carbon nitride is fundamental for affording better catalytic conversion. Due to the electron-rich nature and hydrophilicity of carbon nitride, water adsorption wins over other substrate adsorption leading to dissipation of photogenerated electrons and holes in H_2/O_2 generation.[147] Additionally, electron-rich N-containing sheets remain negatively charged in aqueous media, making adsorption of some biomolecules highly favorable while excluding others. Besides adsorption, nonselective

adsorption of molecules on carbon nitride also promotes an unselective reaction.[148] The conjugated 2D structure of CN also induces irreversible adsorption of some molecules (especially aromatic lignin derivatives) and screening the catalytic center for further reaction results in catalyst poisoning. Surface modification of carbon nitride not only improves product selectivity but also improves the visible absorption, dispersibility in various solvents, charge separation and interaction with cocatalyst counterparts.[112,149] Various surface functionalization approaches have been researched to improve photocatalytic activity by modifying the chemical functional groups on the surface of carbon nitride. For example, the surface chemistry of carbon nitride can be tuned to afford the desired products by introducing acidic sites.[150] The first study of incorporating sulfonate (–SO_3H) groups in carbon nitride frameworks was reported by Varma *et al.* and developed sulfonated carbon nitride (Sg-CN) that can catalyze conversion of sugars to furanics and transesterification of fatty acid to biodiesel.[151,152] Reisner's group had reported a cyanamide surface-functionalized melon-type carbon nitride ($^{NCN}CN_x$) together with a molecular catalyst NiP for selective oxidation of 4-methylbenzyl alcohol (4-MBA) to 4-methylbenzaldehyde (4-MBAD) with concomitant hydrogen evolution.[87] Compared with unfunctionalized carbon nitride, $^{NCN}CN_x$ exhibited improved photocatalytic activity owing to enhanced interaction and charge transfer through the cyanamide moieties of the $^{NCN}CN_x$ and molecular NiP catalyst. Transient absorption spectroscopy (TAS) results demonstrated that the cyanamide groups on the surface of the photocatalyst are more conducive to the catalytic activity of selective substrate oxidation compared with the charge recombination reactions. Importantly, the photoexcited $^{NCN}CN_x$ could accumulate ultralong-lived "trapped electrons", which can be used under dark conditions to produce solar fuel (dark photocatalysis). Interestingly, the same group later adopted $^{NCN}CN_x$ after ultrasonication for coupling conversion of purified and raw lignocellulose samples with hydrogen generation under simulated sunlight.[103] The activated $^{NCN}CN_x$ coupling with different cocatalysts for photoreforming processes maintained high stability over a wide range of pH values under benign aqueous conditions.

Zhang *et al.* reported a modified KOH/KCl modified carbon nitride (AKCN) nanozyme for glucose conversion to gluconic acid accompanied by a peroxidase-mimicking reaction under visible-light irradiation.[153] As shown in Fig. 7a, the three bands at 1000, 1158, and 2152 cm^{-1} of AKCN revealed the terminal –NH_2 groups were replaced by surface hydroxyl groups (–C–OH), while the new band at around 2180 cm^{-1} was attributed to the cyano groups (–C≡N) after the introduction of KCl and KOH. The XRD and XPS results indicated the interaction between K^+/Cl^- and carbon nitride matrix after KCl and KOH modification, thus achieving efficient charge separation between the interlayers, further improving the photocatalytic activity. The structurally modified carbon nitride (AKCN) could convert glucose into gluconic acid and hydrogen peroxide (H_2O_2) under aerobic conditions, which showed a nearly 100% quantum efficiency of H_2O_2 production (Fig. 7b and c). The DFT calculation further predicted the surface hydroxyl group was preferably bonded with the surface carbon atom and the charge difference decreased to 0.06*e*, which was conducive to the charge transfer between adjacent layers (Fig. 7d). Additionally, the surface carbon atom attached to the –OH group carried a more positive charge (1.43*e*), while the neighboring N atom possessed a more negative charge (−1.08*e*) (Fig. 7e). The intrinsic mechanism is illustrated in Fig. 7f. After photoexcitation, the photogenerated holes were preferably captured at N sites bonded with C–OH groups and then abstracted two H atoms to form NH^+ sites through the oxidation of glucose to gluconic acid. Afterward, oxygen molecules reacted with two electrons trapped within the carbon nitride matrix, which simultaneously captured two protons from the NH^+ sites (protonated by glucose oxidation) to finalize the production of H_2O_2 through 1,4-endoperoxide as an intermediate.

Liu *et al.* synthesized an ethyl alcohol group functionalized carbon nitride (UCN-NA) by an *in situ* C–N coupling method for monosaccharide photoreforming into H_2 using a 5 W white LED light.[88] The thermal annealing of urea and *N*-acetylethanolamine (NA) conjugates at 550 °C, leading to partial replacement of terminal –NH_2 groups with ethanol groups (Fig. 8a). The XPS results showed that the intensity of C–C peaks were largely increased after adding NA and the N–C=N peak shifted toward low binding energy, demonstrating the introduction of ethyl alcohol groups which can transfer electrons to the pyridine N in heptazine units (Fig. 8b and c). As shown in Fig. 8d, the relative intensity ratio of the ^{13}C NMR signals for UCN-NA corresponding to C-NH to C–$(N)_3$ was increased and a new peak at 132.2 ppm appeared, further verifying the existence of ethyl alcohol. The ethyl alcohol groups were grafted to CN *via* substituting the terminal amino groups, resulting in enhanced visible-light absorption and improved charge separation as it works as an electron donor. The role of ethyl alcohol groups was further investigated by density functional theory (DFT) calculations. Compared with UCN, a newly-formed impurity level was found within the UCN-NA structure, leading to the formation of an intermediate band (Fig. 8e). The lowest unoccupied molecular orbital (LUMO) of both samples were connected with C–N bonding, while the highest occupied molecular orbital (HOMO) of UCN-NA was mainly located at melem units bonded with the ethyl alcohol group, thus forming an internal electronic field to favor the charge carrier's separation (Fig. 8f and g). Additionally, the edge functionalization favored biomass accessibility on the carbon nitride surface, further improving the photoreforming performance. Specifically, UCN-$NA_{0.5}$ exhibited the maximum hydrogen production rate of 136.9 μmol in D-xylose photoreforming, which was almost 6 times that of pure UCN (23.1 μmol). Later, Liu *et al.* presented an in-plane surface dyadic heterostructure of polymeric carbon nitride using the same organic amine base, *N*-acetylethanolamine (NEA), and dicyandiamide as another precursor.[154] The modified carbon nitride (HCN-NEA) with in-plane surface dyadic hetero-

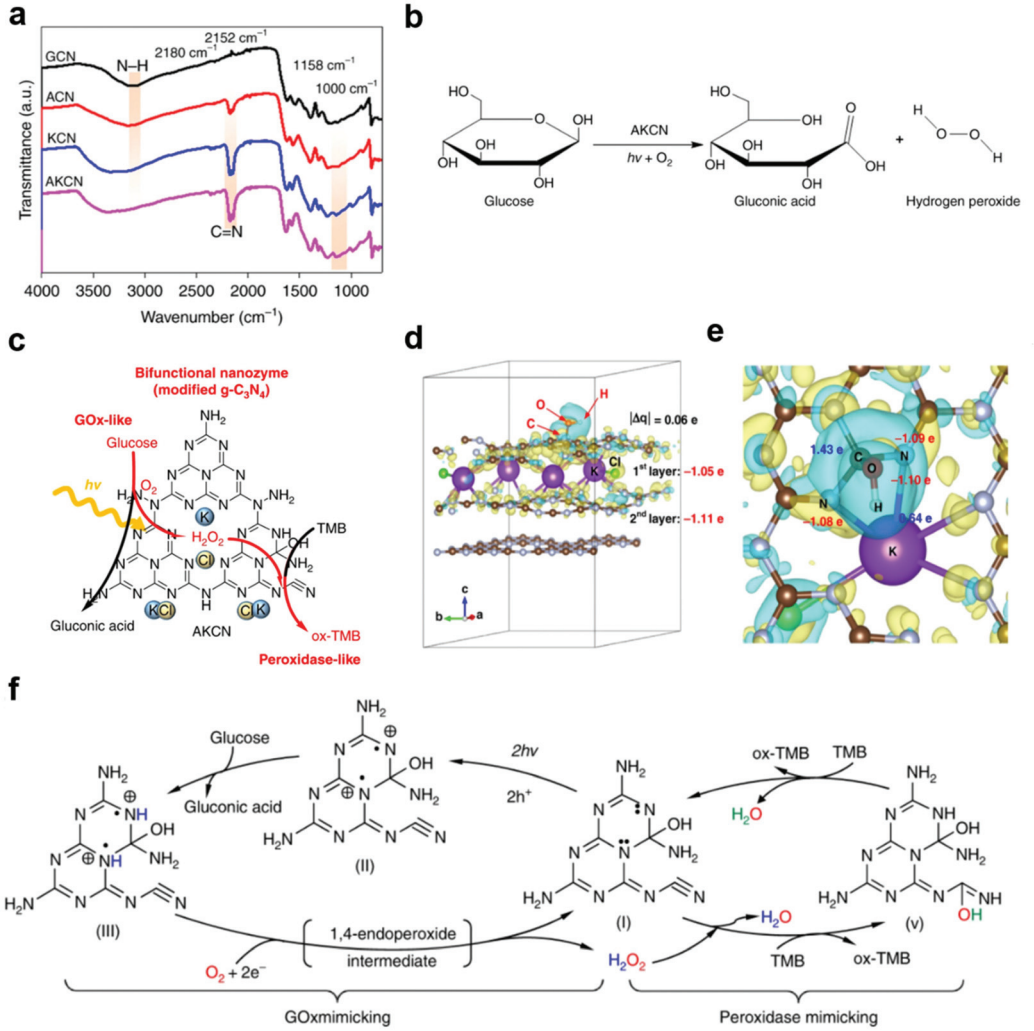

Fig. 7 (a) FTIR spectra of GCN, CAN, KCN and AKCN. (b) Photocatalytic aerobic oxidation of glucose with the concurrent production of H_2O_2 by AKCN. (c) Glucose detection using a synthetic bifunctional nanozyme: photocatalytic aerobic oxidation of glucose with *in situ* production of H_2O_2 on AKCN (modified GCN). (d) Charge distribution of KCl-OH-GCN (*i.e.* AKCN), (e) an enlarged top view of KCl-OH-GCN. (f) The effect of charge redistribution on the promotion of photocatalytic H_2O_2 generation between GCN and AKCN. Reproduced from ref. 153 with permission from Springer Nature, copyright 2019.

structure promotes nucleation of supramolecular complex intermediates resulting in a highly porous structure with a positively shifting band position. When used as a photocatalyst for xylose photoreforming, the HCN-NEA displayed an excellent H_2 evolution rate of 122.77 μmol h^{-1} with an apparent quantum efficiency (AQE) of 7.87% under visible light, which was approximately 15.6 times higher than pristine carbon nitride.

Interestingly, Ilkaeva *et al.* synthesized a polymeric carbon nitride and hydrogen peroxide (PCN-H_2O_2) adduct by thermal treatment of PCN with H_2O_2 at different temperatures for selective oxidation of 5-hydroxymethylfurfural (HMF) to 2,5-furandicarboxaldehyde (FDC) in an aqueous solution under natural solar light.[155] They investigated the effect of temperature on the PCN-H_2O_2 adduct and concluded that it can be stable up to 200 °C in air. The strong hydrogen bonding within the adduct was confirmed by the solid-state NMR that is responsible for the obstacle of the surface amino groups, thus leading to the unselective oxidation of the substrate. Despite the activity of PCN-H_2O_2 decreasing, the elimination of hydroxyl radicals during the photocatalytic process can improve the selectivity of FDC from 45% to 88% with 20% HMF conversion under sunlight. The summary of CN-based photocatalysts for photoreforming of biomass derivatives by surface functionalization is shown in Table 2.

In short, surface functionalization is a promising strategy for the development of CN with dispersibility in various solvents and biomass accessibility. The modification strategy on surface functionalization can boost the interaction between the biomass and CN. On the other hand, it can trigger the intrinsic charge distribution of CN, thus improving the separation of charge carriers and further facilitating the biomass

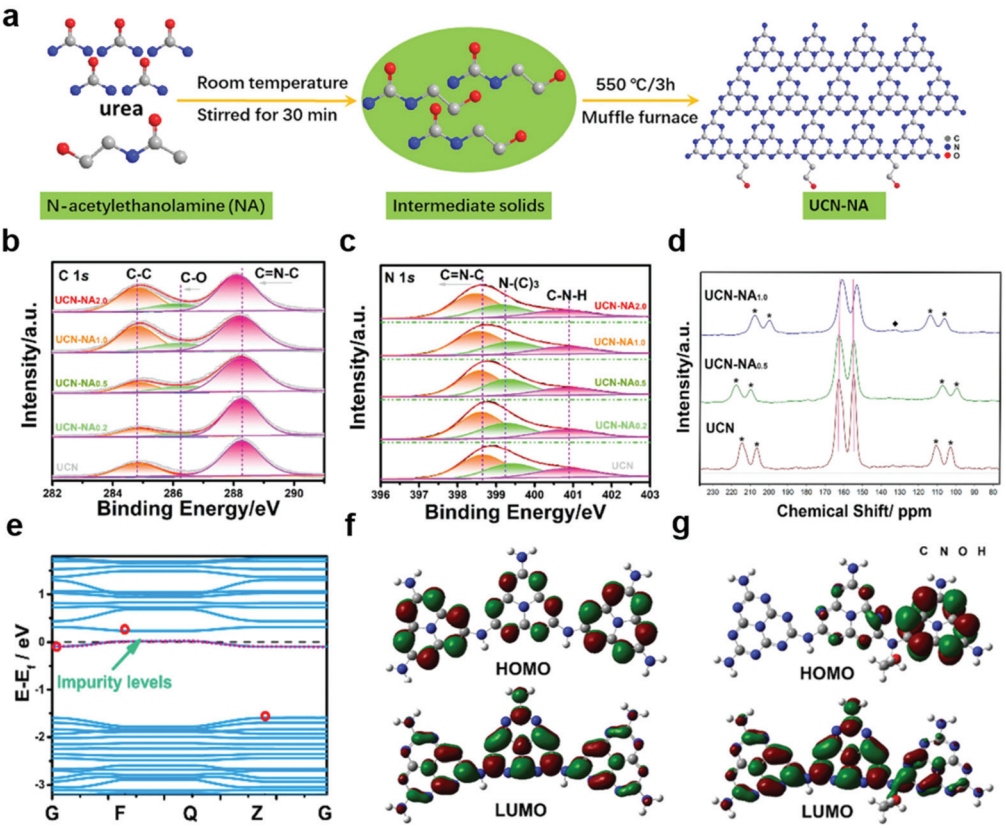

Fig. 8 (a) Schematic illustration of the fabrication of UCN-NA_x. (b) High-resolution XPS C 1s and (c) XPS N 1s patterns of UCN, UCN-$NA_{0.2}$, UCN-$NA_{0.5}$, UCN-$NA_{1.0}$, and UCN-$NA_{2.0}$, respectively. (d) Solid-state ^{13}C magic angle spinning (MAS) NMR spectra of UCN, UCN-$NA_{0.5}$, and UCN-$NA_{1.0}$. * represents the spinning sidebands in the ^{13}C spectra. Calculated band structure of UCN-NA (e) by using DFT. Chemical structures of the polymeric models of UCN (f) and UCN-NA (g) together with the calculated HOMO and LUMO energy levels. Reproduced from ref. 88 with permission from Elsevier, copyright 2020.

photoreforming process. However, the current studies on surface functionalization are mainly focused on H_2 evolution from biomass photoreforming. It is expected to adopt this flexible strategy to graft different surface functional groups to obtain some value-added chemicals by biomass photoreforming of CN-based photocatalysts.

4.3 Elemental doping

Carbon nitride is an excellent photocatalyst due to a moderate band gap of 2.7 eV. However, it absorbs only blue photons below 450–470 nm and suffers from prodigious charge recombination at the interface and trap centers in the less crystalline structures. These issues can be solved by doping carbon nitride with metal or heteroatoms.[156] The next section summarizes the metal and non-metal doping for biomass conversion.

4.3.1 Metal doping. Metal doping inside the tris-*s*-triazine constituted cavity can accommodate a small metal center. Besides this, charge migration from the heptazine center to metal centers leads to better charge separation and improves the effective interaction between carbon nitride sheets and adsorbing substrates.[157,158] For example, the K and Fe modified carbon nitride has been demonstrated to be effective for selective oxidation of benzyl alcohol to benzoin,[159] and 5-hydroxymethylfurfural (HMF) to 2,5-dimethylfuran (DMF),[160] respectively. Recently, single atom catalysts (SACs) comprised of isolated single metal atoms coordinated on active supports emerged as a new frontier in the field of catalysis, photocatalysis and electrocatalysis.[161,162] Due to the unique interaction of metal with support (ensemble effect), SACs can afford an astonishing selectivity (usually higher than ~90%) while utilizing each catalytic site in the catalysis.[163] The past few years have witnessed the development of numerous SACs stabilized on various supports (especially oxides and 2D supports) for many applications such as CO_2 reduction, water splitting and selective biomass conversion.[164,165] For example, TiO_2 supported Pt single atoms in very low concentration (0.04%) can selectively catalyze the transformation of furfuryl alcohol to 2-methylfuran.[166] Sadly, inorganic crystals can accommodate a very diluted concentration of metals in a single atom state and start agglomerating at a high concentration resulting in reduced activity. Although graphene-based M–N–C catalysts can retain relatively higher metal contents, the requirement of high temperature for synthesis under an inert environment is undesirable.[167,168] Interestingly, carbon nitride can accommodate a significantly high concentration of metal in the cavity of

the N-linked heptazine network under mild conditions. The strong coordination of metal with secondary (:NC_2) nitrogen atoms make them stable even under harsh reaction conditions. For example, Tian *et al.* synthesized ruthenium single atom catalysts decorated on mesoporous mpg-C_3N_4 (Ru/mpg-C_3N_4), which can reduce vanillin to 2-methoxy-*p*-cresol with 100% conversion and selectivity under 4 MPa H_2 pressure and 160 °C temperature.[169] Interestingly, the product selectivity can be directed toward vanillyl alcohol at a lower temperature (60 °C) due to the stabilization of intermediate species by single atom sites. At present CN based SACs have only been explored for solar hydrogen generation utilizing biomass derivatives such as benzaldehyde (product of lignin biomass pyrolysis) and lactic acid as a sacrificial donor. For example, Wang *et al.* reported that the synthesis of 0.5 wt% Pt single atom supported on carbon nitride (SA-Pt/g-C_3N_4) can oxidize benzaldehyde to benzoic acid at the VB while reducing protons at the CB.[170] Considering the growing interest of the scientific community in SACs, other works will follow on biomass photoconversion.

4.3.2 Nonmetal doping. The doping of carbon nitride *via* the introduction of heteroatoms such as O, P, B, F, Cl, *etc.* influences the charge distribution in the heptazine, which improves the separation efficiency of charge carriers, extending visible-light absorption and tuning the electronic structure.[171,172] The reason is either due to the breaking of symmetry or the introduction of electrons in π-conjugated networks reducing the band gap and shifting the band position.[173–175] Numerous doping strategies such as using ionic liquids ($BmimPF_6$), heteroatom rich precursors (4-(diphenylphosphino)benzoic acid (4-DPPBA)) and self-doping have been adopted to introduce heteroatoms in the carbon nitride network.[176–179] To ameliorate the photophysical properties, co-doping with two heteroatoms is found to be advantageous. For example, Kumar *et al.* synthesized a P- and F-co-doped carbon nitride (PFCN) using a sol–gel-mediated thermal condensation process.[180] The co-doping resulted in the narrowed band gap, thus leading to superior performance for photoreduction of carbon dioxide into methanol. On the other hand, Brønsted acidity was introduced into the material by P-doping, thus further enhancing the thermal conversion from common carbohydrates (glucose, xylose) into furanics (HMF, furfural). Ma *et al.* reported the photocatalytic oxidation of biomass-derived C_5 and C_6 sugars to lactic acid using a functionalized carbon nitride doped with B and O atoms (B@*m*CN-Y) under visible-light irradiation.[83] The B@*m*CN-Y photocatalyst was synthesized by a facile two-step method using melamine, boric acid and acetic acid precursor calcination at 400 °C for 2 h in air, followed by secondary annealing at 560 °C (Fig. 9a). The TEM images of *m*CN and B@*m*CN-3 exhibited a two-dimensional structure (Fig. 9b and c), and the thickness of B@*m*CN-3 measured by AFM was found to be ~2.3 nm (Fig. 9d and e), which facilitates the mobility of charge carriers during the photocatalytic process. As shown in Fig. 9f, the optical pro-

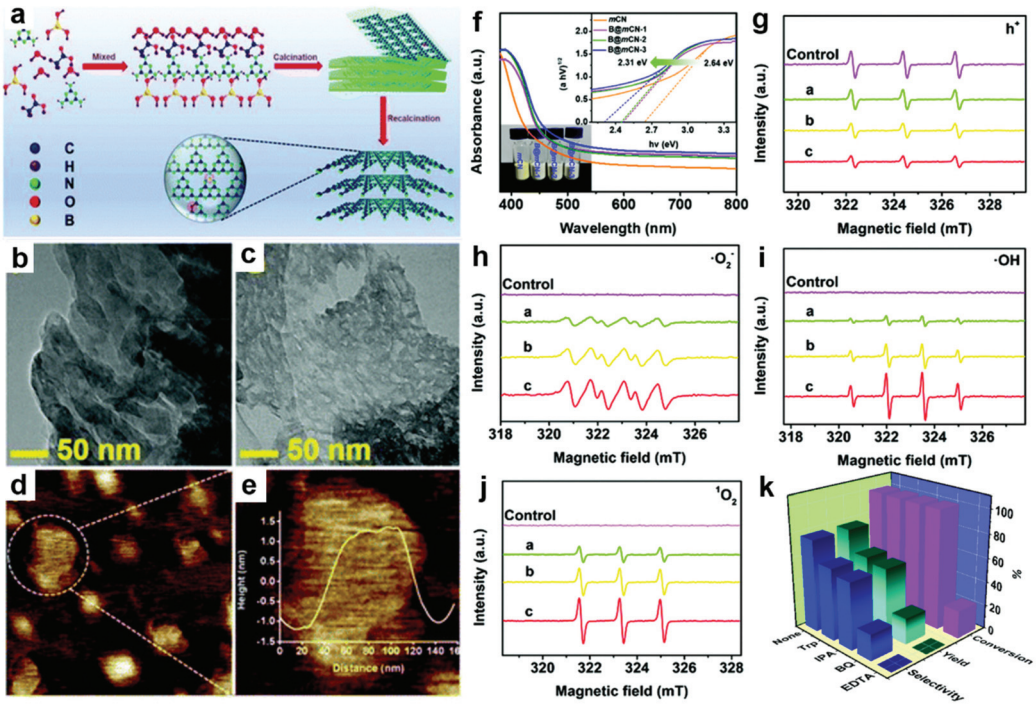

Fig. 9 (a) Schematic of the synthesis of B@mCN-Y. TEM images of (b) *m*CN and (c) B@*m*CN-3. (d and e) AFM images of B@*m*CN-3. (f) UV-vis DRS of the *m*CN, B@*m*CN-1, B@*m*CN-2 and B@*m*CN-3. TEMPO ESR spin-labeling for (g) h^+ and DMPO ESR spin-trapping for (h) $O_2^{\bullet-}$ and (i) $^{\bullet}OH$ as well as TEMPONE ESR spin-labeling for (j) $^1O_2$. (k) The effects of different oxidation active species on the synthesis of lactic acid from glucose. Reproduced from ref. 83 with permission from Royal Society of Chemistry, copyright 2020.

perties of the samples investigated by the UV-vis DRS exhibited an enhanced visible-light absorption and narrowed bandgaps after doping with B and O atoms. The doping not only reduced the bandgap but also improved the separation efficiency of charge carriers, resulting in improved activity for arabinose to lactic acid conversion with a yield of 92.7%. The authors also explored the effects of reaction temperature and solvent concentration on the production of lactic acid during the photoreforming process. After a series of gradient experiments, the optimum reaction temperature and KOH concentration were determined to be 60 °C and 2 mol L^{-1} for the yield of lactic acid, respectively. Moving to the mechanism part, with the increase of doping content, the concentration of h^+, $O_2^{\bullet-}$, $^{\bullet}OH$ and $^1O_2$ was increased as demonstrated in EPR measurement (Fig. 9g–j). A series of control experiments performed to clarify the effects of oxidative species on the yield of lactic acid suggest that h^+ played a major role in the photoreforming reactions, while the other active species like $^1O_2$, $^{\bullet}OH$ and $O_2^{\bullet-}$ played an auxiliary role in the process (Fig. 9k). The catalyst remained stable and recyclable for up to 11 cycles. Additionally, the one-thousand-fold scale-up experiment afforded a 68.6% yield and 89.0% conversion under room temperature and sunlight irradiation. In another study, Ma *et al.* reported an ultrathin porous O-doped carbon nitride (*Ut*-OCN) for lactic acid generation from different biomass-based monosaccharides under visible-light irradiation.[104] The *Ut*-OCN photocatalyst exhibited tunable band gaps and lower PL intensity, leading to increased visible-light absorption range and improved separation efficiency of charge carriers. Using *Ut*-OCN photocatalysts, a remarkable 89.7% yield of lactic acid was achieved. Although all the oxidative active species (h^+, $^1O_2$, $^{\bullet}OH$ and $O_2^{\bullet-}$) contributed to lactic acid production, $O_2^{\bullet-}$ was the dominant reactive species responsible for the oxidation process. Moreover, the photocatalyst was reusable after 10 cycling experiments. The scalability of catalysts to implement at the industrial scale was tested by increasing the reaction proportion one-thousand-times manifesting the potential of lactic acid production through this photocatalytic system. Recently, the same group demonstrated P-doped carbon nitride grafted with sulfonic acid groups (P@CN-SO_3H) could convert xylose into xylonic acid with a yield of 88.1% under visible-light irradiation.[181] The summary of CN-based photocatalysts for photoreforming of biomass derivatives by elemental doping is shown in Table 3.

To sum up, elemental doping indeed plays a significant role in tuning the electronic structure of CN for biomass photoreforming. The element-doped CNs not only enhance the visible-light absorption, but also improve the separation efficiency of charge carriers, thus resulting in improved activity for biomass photoreforming, even for the one-thousand-fold scale-up experiment. However, current studies on elemental doping strategy mainly focus on the alkaline conditions for biomass photoreforming, which is less environment-friendly. It is expected that element-doped CNs would further be applied in mild conditions like neutral solutions for biomass photoreforming.

4.4 Other modifications

Apart from the approaches mentioned above, many other modifications have been investigated to improve the photoreforming efficiency. In the bulk carbon nitride, significant surface/active sites remain unexposed due to intense stacking between hydrogen-bonded sheets. The improvement of surface area and porosity is essential for the adsorption of biomass. To overcome such challenges, several surface area modification approaches, such as solvent and acid exfoliation, adopting two or more different precursors, using hard and soft templates as structure determining agents, and the use of hydrogen-bonded macromolecular aggregates, have already been developed.[182–184]

4.4.1 Surface area improvement using hard templates. Silica is the most used hard templating material for the synthesis of high surface area nano/mesoporous carbon nitride due to facile synthesis, the possibility of controlling microstructures using a wide variety of ordered silica structures such as SBA-15 and MCM-41 and the formation of resilient structures which do not collapse after the removal of template materials.[185,186] Vinu *et al.* pioneered the synthesis of N-rich triazine (C_3N_3)-based ordered carbon nitride structures using such mesoporous silica.[187] For the heptazine (C_6N_7)-based carbon nitride, maintaining ordered mesoporous channels remains challenging due to high-temperature synthesis distorting the morphology. However, such an approach certainly allows the attainment of high surface area and improves photoactivity. Liu *et al.* reported a mesoporous graphitic carbon nitride (mpg-C_3N_4) for photocleavage of C–C bonds in lignin models to aromatic aldehydes (acids) and phenolic esters under visible-light irradiation.[188] They adopted a hard-template method using tetraethyl orthosilicate (TEOS) to obtain mpg-C_3N_4 with a large specific surface area of 206.5 m^2 g^{-1} that increases the concentration of active sites available for the photocatalytic reactions. The common oxidation products of β-O-4 linkage containing lignin model 2-phenoxy-1-phenylethanol (molecule 1) possessing C_α–OH, C_α–C_β, and C_β–O bonds are presented in Fig. 10a. The DFT calculations were adopted to demonstrate the π–π stacking interactions between mpg-C_3N_4 and lignin models. After optimizing the interaction models, a model that had two benzene rings of molecules almost parallel to the triazine rings of mpg-C_3N_4 with higher absorption energy of −0.92 eV was identified (Fig. 10b and c). This absorption pattern belonged to π–π stacking interactions, further enhancing the molecule activation and charge transfer between electron-rich C_3N_4 and some aromatic molecules. As shown in Fig. 10d, a possible mechanism for the conversion of lignin molecule 1 using mpg-C_3N_4 under photocatalysis was proposed. The oxidation of model molecule 1 proceeds through several steps, such as deprotonation of C_β, formation of peroxide intermediate, C_α–C_β and O–O bond cleavage, that finally yield major products (benzaldehyde and phenyl formate). Another similar method was adopted by Battula *et al.*,[189] which developed a porous carbon nitride (SGCN) for selective oxidation of 5-hydroxymethylfurfural (HMF) to 2,5-

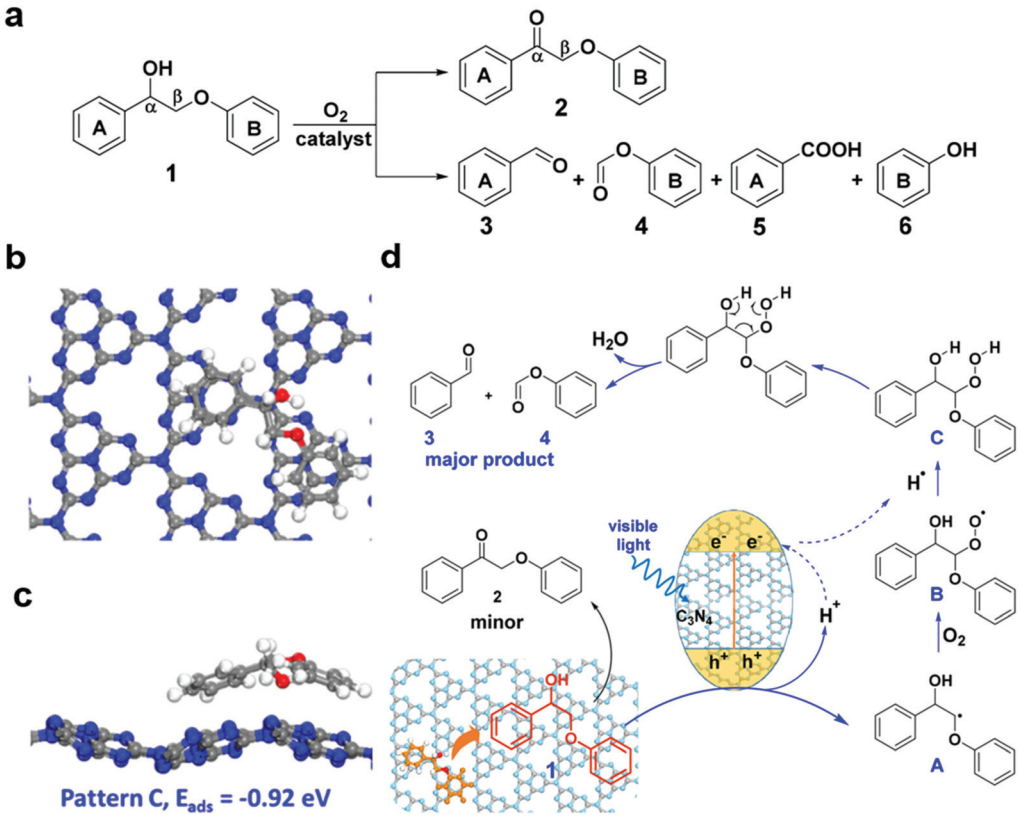

Fig. 10 (a) General oxidative products of 2-phenoxy-1-phenylethanol. (b and c) Optimized interaction patterns (top view and side view) and adsorption energies of substrate molecule 1 adsorbed on a corrugated C_3N_4 surface (color scheme: H, white; C, gray; N, blue; O, red). (d) Proposed mechanism of mpg-C_3N_4 catalyzed transformation of molecule 1. Reproduced from ref. 188 with permission from ACS Publications, copyright 2018.

diformylfuran (DFF) integrated with H_2 production under visible-light irradiation. The SGCN achieved over 99% selectivity and 38.4% yield of DFF along with an H_2 generation rate of 36 μmol h^{-1} m^{-2}. Additionally, the mesoporous carbon nitride (M-CNU) prepared by hard template methods was adopted for the photooxidation of tetrahydrofurfuryl alcohol (THFA) into γ-butyrolactone (GBL) through a 390 nm LED light.[190]

4.4.2 Surface area improvement using soft templates. Regardless of the hard template-assisted synthesis of porous carbon nitride materials sustaining a robust structure, the complete removal of silica using harsh HF residual silica is not economical, while residual silica also clogs many pores. To avoid such circumstances, the use of soft templates is impregnable. Many organic surfactants, including some large tail molecules, have been utilized to get porous carbon nitride with ordered mesopores.[191,192] Surfactants are proven to be more alluring options as surfactants also enhance the dispersibility of materials. In a recent report, Kumar *et al.* synthesized a high surface area (260.93 m^2 g^{-1}) P- and F-co-doped carbon nitride (PFCN) using CTAB and TEOS as soft and hard templating agents, respectively.[180] Due to the co-doping, the bandgap of PFCN was narrowed up to 1.8 eV and excellent methanol formation from CO_2 was observed. Beyond the photocatalytic activity, the scope of catalysts for thermal chemocatalytic conversion of biomass was also tested. The PFCN was found to be an active catalyst for the conversion of sugars (glucose, xylose) to furanics (HMF) at relatively mild conditions. Wu *et al.* adopted a water treatment strategy in which water vapors work as a soft template for the synthesis of porous metal-free graphitic carbon nitride (g-C_3N_4) photocatalysts.[193] The water treatment followed by heating refined the pore structure, thus resulting in a largely increased specific surface area (123.9 m^2 g^{-1}) compared with pure g-C_3N_4 (11.4 m^2 g^{-1}). Moreover, enhanced light-harvest ability and improved separation efficiency of charge carriers were achieved according to UV-vis and PL spectra. Hence, the modified g-C_3N_4 exhibited the highest 2,5-diformylfuran (DFF) selectivity of 85.6% with 31.2% of 5-hydroxymethylfurfural (HMF) conversion under visible-light illumination.

4.4.3 Activity improvement by thermochemical approaches. Krivtsov *et al.* reported a modified g-C_3N_4 (MCN_520) by a thermal exfoliation procedure for photocatalytic oxidation of 5-hydroxymethyl-2-furfural (HMF) to 2,5-furandicarboxaldehyde (FDC) under real outdoor illumination.[194] The thermal exfoliation increased the specific surface area, which not only accelerated the rate of reaction but also removed the uncondensed $-NH_2$ groups from the surface of g-C_3N_4. The high selectivity of HMF to DFC was attributed to the formation of $O_2^{\bullet-}$ radicals instead of the unselective $^\bullet$OH.

Later, Akhundi *et al.* adopted different methodologies like sonochemical treatment, hydrothermal and ball milling, and thermo-exfoliation for the selective oxidation of HMF to FDC under natural solar light.[195] It was found that the HMF conversion and FDC selectivity could be achieved by the exfoliation of carbon nitride, while the thermal exfoliation treatments performed the best photocatalytic activity (TE-520). Speltini *et al.* synthesized a chemical modified g-C_3N_4 using the acid treatment for photocatalytic H_2 evolution assisted by glucose conversion under natural solar light.[196] The g-C_3N_4 treated with hot HNO_3 aqueous solution (*o*-g-C_3N_4) exhibited 26 times higher photocatalytic activity compared with the pristine g-C_3N_4. Additionally, they indicated the versatility of *o*-g-C_3N_4 that could be applied in raw environmental waters such as river water and seawater.

Pichler *et al.* reported a cyanamide-functionalized carbon nitride ($^{NCN}CN_x$) for photoreforming of biomass in metal salt hydrate (MSH) solutions under simulated sunlight.[197] Lignocellulosic biomass derivatives could be depolymerized into soluble sugars in proper MSH solutions under mild conditions. For instance, Li^+ derived from LiBr interacted strongly with water molecules, thus causing acidity which depolymerizes cellulose, while the Br^- facilitated hydrogen-bonding interactions within the cellulose chain. The MSH medium created favorable accessibility between the substrate and photocatalyst, thereby achieving higher efficiency of biomass conversion. The summary of CN-based photocatalysts for photoreforming of biomass derivatives by other modifications is shown in Table 4.

In summary, the other modifications including hard-/soft-template, chemical modification and solvent modulation have been successfully demonstrated for biomass photoreforming on CN-based photocatalysts. Hard-/soft-template and chemical modifications can achieve higher specific surface area and porosity, which is important for the absorption of biomolecules. In addition, the increased specific surface area can also expose more surface active sites, thus improving the separation efficiency of charge carriers to further boost the biomass photoreforming process. Solvent modulation using MSH solution can favor the biomass accessibility by metal ions under mild conditions, thus further facilitating biomass photoreforming. However, there are a few other modifications like morphology design or N-rich precursors reported on the application of CN-based photocatalysts to biomass photoreforming. Since this research field is growing so fast, it is anticipated that other modification strategies for CN-based photocatalysts to be applied in biomass photoreforming will be reported in the future.

5 Conclusions and perspectives

Technologies to capture solar energy in various energy forms, including solar to electrical (STE) in photovoltaics and solar to chemicals (STC) in photocatalysis, have gained significant interest in the past few decades.[198,199] While STE is mature technology and deployed on the industrial scale, the use of photocatalysis remains confined to laboratory-scale or waste water treatment due to the unavailability of an efficient widely absorbing photocatalytic material with ideal redox band edges. Even though a few semiconductor materials meet such requirements, stability, short carrier migration length and processability remain a challenge. Carbon nitride provides optimism in the future of photocatalysis due to its intriguing physicochemical properties and lack of photocorrosion. Due to the low cost, high stability, unique conduction and valence bands, as well as feasible structure adjustability by structural manipulation, carbon nitride-based materials have been widely investigated for various applications including solar fuel generation from water and CO_2. Photosynthetically stored energy in biomass molecules (produced from CO_2 and water) increases the energy of the molecules, easing their activation using photocatalysts. The photoreforming of biomass not only proceeds at low energy inputs but can also produce two chemicals at both conduction and valence bands. The present review discusses the state-of-the-art research progress of carbon nitride-based photocatalysts for photoreforming of biomass derivatives focusing on hybrid heterostructures, surface functionalization, elemental doping, and various other modification strategies. Decoration of carbon nitride with metal complexes, metal nanoparticles, and semiconductors can achieve highly efficient charge separation and more active sites for biomass photoreforming. Adding active groups on the surface of CN not only boosts the interaction with biomass but can also trigger charge distribution of the CN matrix, thus improving the separation of charge carriers and further facilitating the biomass photoreforming process. The modification strategy on elemental doping can enhance the visible-light absorption and improve separation efficiency of charge carriers as well, resulting in promoted activity for biomass photoreforming. Additionally, the specific surface area modification populates the active sites and porosity, as well as the accessibility of biomass molecules. The hybrid heterostructures demonstrated potential in photoreforming of HMF, monosaccharides, and even cellulose. Apart from conventional thermocatalytic biomass-derived chemicals, the CN-based photocatalysts could convert biomass into high-value fine chemicals such as aldehydes and mono/di-carboxylic acids, *etc*. In some cases, acid treatment or solvent modulation achieves hydrogen production coupled with glucose photoreforming.

There are some critical challenges that should be addressed in the future to make photoreforming technology viable. First, the hydrogen production efficiency and biomass conversion rate of photoreforming processes are too low and restrained in the micromolar regime. Second, whether the high selectivity and separation of target products in biomass conversion can be achieved is very significant. For instance, most of the reported studies using CN-based photocatalysts achieve relatively low selectivity and yield in biomass conversion, which leads to challenges with target product separation. Third, the mechanism of biomass valorization reactions using CN-based photocatalysts is still unclear, especially for native ligno-

cellulosic biomass. Employing advanced sophisticated tools such as transient absorption spectroscopy (TAS), electron paramagnetic resonance (EPR) and theoretical calculations such as DFT can put forth light on a deeper understanding of biomass photoreforming mechanisms. Last but not least, the studies regarding native lignocellulosic biomass are in their infancy. Most of the current studies adopt model compounds like glucose or HMF instead of real biomass due to its low accessibility and complex physicochemical properties. Therefore, the photoreforming of native lignocellulosic biomass by CN-based photocatalysts into value-added products remains an enormous challenge. The future holds the challenges of developing robust photocatalyst and processing protocols for converting complex biomass into value-added chemicals.

Given the reported pieces of literature, significant progress in the CN-based photocatalysts with great potential to be applied in biomass valorization has been made. Besides the aforementioned modification strategies, it is anticipated that other modifications like morphology design for CN-based photocatalysts to be applied in biomass photoreforming will be reported in the future. The information in this review aims to provide effective guidance for the future design of CN-based photocatalysts in biomass valorization to promote the hydrogen evolution efficiency and the selectivity of target products. Although some issues and challenges remain currently, we believe a bright future in the design and applications of CN-based photocatalysts for photoreforming of biomass derivatives is coming.

Conflicts of interest

The authors declare no conflict of interest.

Acknowledgements

The completion of this research is supported by the Canada First Research Excellence Fund (CFREF).

Notes and references

1 L. Wang, W. Chen, D. Zhang, Y. Du, R. Amal, S. Qiao, J. Wu and Z. Yin, *Chem. Soc. Rev.*, 2019, **48**, 5310–5349.
2 Y. Dong, P. Duchesne, A. Mohan, K. K. Ghuman, P. Kant, L. Hurtado, U. Ulmer, J. Y. Loh, A. A. Tountas and L. Wang, *Chem. Soc. Rev.*, 2020, **49**, 5648–5663.
3 P. Gallezot, *Chem. Soc. Rev.*, 2012, **41**, 1538–1558.
4 R. A. Sheldon, *Green Chem.*, 2014, **16**, 950–963.
5 S. Wang, G. Dai, H. Yang and Z. Luo, *Prog. Energy Combust. Sci.*, 2017, **62**, 33–86.
6 X. Liu, X. Duan, W. Wei, S. Wang and B.-J. Ni, *Green Chem.*, 2019, **21**, 4266–4289.
7 X. Wu, N. Luo, S. Xie, H. Zhang, Q. Zhang, F. Wang and Y. Wang, *Chem. Soc. Rev.*, 2020, **49**, 6198–6223.
8 A. Hendriks and G. Zeeman, *Bioresour. Technol.*, 2009, **100**, 10–18.
9 N. Jiang, L. Lyu, G. Yu, L. Zhang and C. Hu, *J. Mater. Chem.*, 2018, **6**, 17819–17828.
10 Z. Xiang, W. Han, J. Deng, W. Zhu, Y. Zhang and H. Wang, *ChemSusChem*, 2020, **13**, 4199–4213.
11 L. I. Granone, F. Sieland, N. Zheng, R. Dillert and D. W. Bahnemann, *Green Chem.*, 2018, **20**, 1169–1192.
12 T. Butburee, P. Chakthranont, C. Phawa and K. Faungnawakij, *ChemCatChem*, 2020, **12**, 1873–1890.
13 P. Phitsuwan, K. Sakka and K. Ratanakhanokchai, *Biomass Bioenergy*, 2013, **58**, 390–405.
14 Y. Zheng, J. Zhao, F. Xu and Y. Li, *Prog. Energy Combust. Sci.*, 2014, **42**, 35–53.
15 L. Yang, F. Xu, X. Ge and Y. Li, *Renewable Sustainable Energy Rev.*, 2015, **44**, 824–834.
16 H. Zhao, C. F. Li, X. Yong, P. Kumar, B. Palma, Z. Y. Hu, G. Van Tendeloo, S. Siahrostami, S. Larter, D. Zheng, S. Wang, Z. Chen, M. G. Kibria and J. Hu, *iScience*, 2021, **24**, 102109.
17 P. Parthasarathy and K. S. Narayanan, *Renewable Energy*, 2014, **66**, 570–579.
18 D. D. Laskar, M. P. Tucker, X. Chen, G. L. Helms and B. Yang, *Green Chem.*, 2014, **16**, 897–910.
19 D. Wang, B. Wang, Y. Ding, Q. Yuan, H. Wu, Y. Guan and P. Wu, *Chem. Commun.*, 2017, **53**, 10172–10175.
20 S. Dutta, K. Iris, D. C. Tsang, Y. H. Ng, Y. S. Ok, J. Sherwood and J. H. Clark, *Chem. Eng. J.*, 2019, **372**, 992–1006.
21 W. Luo, W. Cao, P. C. Bruijnincx, L. Lin, A. Wang and T. Zhang, *Green Chem.*, 2019, **21**, 3744–3768.
22 C. Mondelli, G. Gözaydın, N. Yan and J. Pérez-Ramírez, *Chem. Soc. Rev.*, 2020, **49**, 3764–3782.
23 J. Pang, J. Sun, M. Zheng, H. Li, Y. Wang and T. Zhang, *Appl. Catal., B*, 2019, **254**, 510–522.
24 K. J. Smith, *Curr. Opin. Green Sustainable*, 2020, **22**, 47–53.
25 Y. N. Regmi, B. Rogers, N. Labbé and S. C. Chmely, *ACS Sustainable Chem. Eng.*, 2017, **5**, 7751–7758.
26 Y. Yang, L. Chen, Y. Chen, W. Liu, H. Feng, B. Wang, X. Zhang and M. Wei, *Green Chem.*, 2019, **21**, 5352–5362.
27 D. A. Constantinou and A. M. Efstathiou, *Appl. Catal., B*, 2010, **96**, 276–289.
28 L. Kong, Y. Ji, Z. Dang, J. Yan, P. Li, Y. Li and S. F. Liu, *Adv. Funct. Mater.*, 2018, **28**, 1800668.
29 J. Fu, K. Liu, K. Jiang, H. Li, P. An, W. Li, N. Zhang, H. Li, X. Xu, H. Zhou, D. Tang, X. Wang, X. Qiu and M. Liu, *Adv. Sci.*, 2019, **6**, 1900796.
30 C. H. Choi, L. Lin, S. Gim, S. Lee, H. Kim, X. Wang and W. Choi, *ACS Catal.*, 2018, **8**, 4241–4256.
31 H. Liu, S. Ma, L. Shao, H. Liu, Q. Gao, B. Li, H. Fu, S. Fu, H. Ye and F. Zhao, *Appl. Catal., B*, 2020, **261**, 118201.
32 F. Parrino, M. Bellardita, E. I. García-López, G. Marcì, V. Loddo and L. Palmisano, *ACS Catal.*, 2018, **8**, 11191–11225.
33 M. F. Kuehnel and E. Reisner, *Angew. Chem., Int. Ed.*, 2018, **57**, 3290–3296.

34 S. Kampouri and K. C. Stylianou, *ACS Catal.*, 2019, **9**, 4247–4270.
35 E. Reisner, *Angew. Chem., Int. Ed.*, 2019, **58**, 3656–3657.
36 Z. Gong, G. Yang, J. Song, P. Zheng, J. Liu, W. Zhu, L. Huang, L. Chen, X. Luo and L. Shuai, *Bioresour. Bioprocess.*, 2021, **8**, 1–14.
37 V. Nair, P. Dhar and R. Vinu, *RSC Adv.*, 2016, **6**, 18204–18216.
38 S. S. Hassan, G. A. Williams and A. K. Jaiswal, *Bioresour. Technol.*, 2018, **262**, 310–318.
39 G. Han, Y.-H. Jin, R. A. Burgess, N. E. Dickenson, X.-M. Cao and Y. Sun, *J. Am. Chem. Soc.*, 2017, **139**, 15584–15587.
40 D. W. Wakerley, M. F. Kuehnel, K. L. Orchard, K. H. Ly, T. E. Rosser and E. Reisner, *Nat. Energy*, 2017, **2**, 1–9.
41 X. Wu, X. Fan, S. Xie, J. Lin, J. Cheng, Q. Zhang, L. Chen and Y. Wang, *Nat. Catal.*, 2018, **1**, 772–780.
42 M. Wang, M. Liu, J. Lu and F. Wang, *Nat. Commun.*, 2020, **11**, 1083.
43 H. Zhao, P. Liu, X. Wu, A. Wang, D. Zheng, S. Wang, Z. Chen, S. Larter, Y. Li, B.-L. Su, M. G. Kibria and J. Hu, *Appl. Catal., B*, 2021, **291**, 120055.
44 N. Roy, Y. Sohn and D. Pradhan, *ACS Nano*, 2013, **7**, 2532–2540.
45 H. Huang, B. Dai, W. Wang, C. Lu, J. Kou, Y. Ni, L. Wang and Z. Xu, *Nano Lett.*, 2017, **17**, 3803–3808.
46 J. Zhang, Z. Yu, Z. Gao, H. Ge, S. Zhao, C. Chen, S. Chen, X. Tong, M. Wang and Z. Zheng, *Angew. Chem., Int. Ed.*, 2017, **56**, 816–820.
47 C. Bie, B. Zhu, F. Xu, L. Zhang and J. Yu, *Adv. Mater.*, 2019, **31**, 1902868.
48 X. Wu, J. Li, S. Xie, P. Duan, H. Zhang, J. Feng, Q. Zhang, J. Cheng and Y. Wang, *Chem*, 2020, **6**, 3038–3053.
49 C. Li, H. Wang, S. B. Naghadeh, J. Z. Zhang and P. Fang, *Appl. Catal., B*, 2018, **227**, 229–239.
50 H.-F. Ye, R. Shi, X. Yang, W.-F. Fu and Y. Chen, *Appl. Catal., B*, 2018, **233**, 70–79.
51 Y.-H. Li, F. Zhang, Y. Chen, J.-Y. Li and Y.-J. Xu, *Green Chem.*, 2020, **22**, 163–169.
52 N. Luo, M. Wang, H. Li, J. Zhang, T. Hou, H. Chen, X. Zhang, J. Lu and F. Wang, *ACS Catal.*, 2017, **7**, 4571–4580.
53 S. Chen, T. T. Qian, L. L. Ling, W. Zhang, B. B. Gong and H. Jiang, *ChemSusChem*, 2020, **13**, 5507–5515.
54 H. Zhao, C.-F. Li, L.-Y. Liu, B. Palma, Z.-Y. Hu, S. Renneckar, S. Larter, Y. Li, M. G. Kibria and J. Hu, *J. Colloid Interface Sci.*, 2021, **585**, 694–704.
55 L. Shiamala, K. Alamelu, V. Raja and J. Ali, *J. Environ. Chem. Eng.*, 2018, **6**, 3306–3321.
56 S. Dhingra, T. Chhabra, V. Krishnan and C. Nagaraja, *ACS Appl. Energy Mater.*, 2020, **3**, 7138–7148.
57 A. Kudo and Y. Miseki, *Chem. Soc. Rev.*, 2009, **38**, 253–278.
58 S. Cao, J. Low, J. Yu and M. Jaroniec, *Adv. Mater.*, 2015, **27**, 2150–2176.
59 X. Chang, T. Wang and J. Gong, *Energy Environ. Sci.*, 2016, **9**, 2177–2196.
60 A. Thomas, A. Fischer, F. Goettmann, M. Antonietti, J.-O. Müller, R. Schlögl and J. M. Carlsson, *J. Mater. Chem.*, 2008, **18**, 4893–4908.
61 Y. Wang, H. Li, J. Yao, X. Wang and M. Antonietti, *Chem. Sci.*, 2011, **2**, 446–450.
62 Y. Wang, X. Wang and M. Antonietti, *Angew. Chem., Int. Ed.*, 2012, **51**, 68–89.
63 P. Xia, S. Cao, B. Zhu, M. Liu, M. Shi, J. Yu and Y. Zhang, *Angew. Chem.*, 2020, **59**, 5218–5225.
64 P. Kumar, E. Vahidzadeh, U. K. Thakur, P. Kar, K. M. Alam, A. Goswami, N. Mahdi, K. Cui, G. M. Bernard and V. K. Michaelis, *J. Am. Chem. Soc.*, 2019, **141**, 5415–5436.
65 I. Y. Kim, S. Kim, S. Premkumar, J. H. Yang, S. Umapathy and A. Vinu, *Small*, 2020, **16**, 1903572.
66 B. Mortazavi, F. Shojaei, M. Shahrokhi, M. Azizi, T. Rabczuk, A. V. Shapeev and X. Zhuang, *Carbon*, 2020, **167**, 40–50.
67 S. Shen, L. Zhao, X. Guan and L. Guo, *J. Phys. Chem. Solids*, 2012, **73**, 79–83.
68 X. Li, J. Yu, M. Jaroniec and X. Chen, *Chem. Rev.*, 2019, **119**, 3962–4179.
69 B. Xia, Y. Zhang, B. Shi, J. Ran, K. Davey and S. Z. Qiao, *Small Methods*, 2020, **4**, 2000063.
70 U. Nwosu, A. Wang, B. Palma, H. Zhao, M. A. Khan, M. Kibria and J. Hu, *Renewable Sustainable Energy Rev.*, 2021, **148**, 111266.
71 H. Hao, L. Zhang, W. Wang, S. Qiao and X. Liu, *ACS Sustainable Chem. Eng.*, 2019, **7**, 10501–10508.
72 L. Zhang, D. Jiang, R. M. Irfan, S. Tang, X. Chen and P. Du, *J. Energy Chem.*, 2019, **30**, 71–77.
73 C. Y. Toe, C. Tsounis, J. Zhang, H. Masood, D. Gunawan, J. Scott and R. Amal, *Energy Environ. Sci.*, 2021, **14**, 1140–1175.
74 J. C. Colmenares and R. Luque, *Chem. Soc. Rev.*, 2014, **43**, 765–778.
75 X. Lu, S. Xie, H. Yang, Y. Tong and H. Ji, *Chem. Soc. Rev.*, 2014, **43**, 7581–7593.
76 B. Zhou, J. Song, Z. Zhang, Z. Jiang, P. Zhang and B. Han, *Green Chem.*, 2017, **19**, 1075–1081.
77 X. Ruan, Y. Sun, W. Du, Y. Tang, Q. Liu, Z. Zhang, W. Doherty, R. L. Frost, G. Qian and D. C. Tsang, *Bioresour. Technol.*, 2019, **281**, 457–468.
78 A. S. Roy, A. C. Poulose, A. Bakandritsos, R. S. Varma and M. Otyepka, *Appl. Mater. Today*, 2021, **23**, 101053.
79 A. Vijeta and E. Reisner, *Chem. Commun.*, 2019, **55**, 14007–14010.
80 R. S. A. Ribeiro, L. E. M. Ferreira, V. Rossa, C. G. S. Lima, M. W. Paixão, R. S. Varma and T. M. Lima, *ChemSusChem*, 2020, **13**, 3992–4004.
81 S. Mitroka, S. Zimmeck, D. Troya and J. M. Tanko, *J. Am. Chem. Soc.*, 2010, **132**, 2907–2913.
82 B. Long, Z. Ding and X. Wang, *ChemSusChem*, 2013, **6**, 2074–2078.
83 J. Ma, Y. Li, D. Jin, Z. Ali, G. Jiao, J. Zhang, S. Wang and R. Sun, *Green Chem.*, 2020, **22**, 6384–6392.

84 X. Wu, H. Zhao, M. A. Khan, P. Maity, T. Al-Attas, S. Larter, Q. Yong, O. F. Mohammed, M. G. Kibria and J. Hu, *ACS Sustainable Chem. Eng.*, 2020, **8**, 15772–15781.
85 S. Verma, R. B. N. Baig, M. N. Nadagouda and R. S. Varma, *Green Chem.*, 2016, **18**, 1327–1331.
86 S. Yu, S. Zhang, K. Li, Q. Yang, M. Wang, D. Cai, T. Tan and B. Chen, *ACS Sustainable Chem. Eng.*, 2020, **8**, 15980–15988.
87 H. Kasap, C. A. Caputo, B. C. M. Martindale, R. Godin, V. W.-h. Lau, B. V. Lotsch, J. R. Durrant and E. Reisner, *J. Am. Chem. Soc.*, 2016, **138**, 9183–9192.
88 Q. Liu, L. Wei, Q. Xi, Y. Lei and F. Wang, *Chem. Eng. J.*, 2020, **383**, 123792.
89 W. Zou, Y. Shao, Y. Pu, Y. Luo, J. Sun, K. Ma, C. Tang, F. Gao and L. Dong, *Appl. Catal., B*, 2017, **218**, 51–59.
90 Y. Guo, P. Niu, Y. Liu, Y. Ouyang, D. Li, T. Zhai, H. Li and Y. Cui, *Adv. Mater.*, 2019, **31**, 1900342.
91 Y. Kang, Y. Yang, L. C. Yin, X. Kang, L. Wang, G. Liu and H. M. Cheng, *Adv. Mater.*, 2016, **28**, 6471–6477.
92 P. Kumar, R. Boukherroub and K. Shankar, *J. Mater. Chem. A*, 2018, **6**, 12876–12931.
93 G. Liao, Y. Gong, L. Zhang, H. Gao, G.-J. Yang and B. Fang, *Energy Environ. Sci.*, 2019, **12**, 2080–2147.
94 L. Lin, Z. Yu and X. Wang, *Angew. Chem., Int. Ed.*, 2019, **58**, 6164–6175.
95 Y. Wang, S. Z. F. Phua, G. Dong, X. Liu, B. He, Q. Zhai, Y. Li, C. Zheng, H. Quan, Z. Li and Y. Zhao, *Chem*, 2019, **5**, 2775–2813.
96 S. N. Talapaneni, G. Singh, I. Y. Kim, K. AlBahily, A. H. Al-Muhtaseb, A. S. Karakoti, E. Tavakkoli and A. Vinu, *Adv. Mater.*, 2020, **32**, 1904635.
97 P. Niu and L. Li, *Chem*, 2020, **6**, 2439–2441.
98 C. Zhao, Z. Chen, R. Shi, X. Yang and T. Zhang, *Adv. Mater.*, 2020, **32**, 1907296.
99 J. Ran, W. Guo, H. Wang, B. Zhu, J. Yu and S. Z. Qiao, *Adv. Mater.*, 2018, **30**, 1800128.
100 H. Xu, X. She, T. Fei, Y. Song, D. Liu, H. Li, X. Yang, J. Yang, H. Li, L. Song, P. M. Ajayan and J. Wu, *ACS Nano*, 2019, **13**, 11294–11302.
101 P. Huang, J. Huang, S. A. Pantovich, A. D. Carl, T. G. Fenton, C. A. Caputo, R. L. Grimm, A. I. Frenkel and G. Li, *J. Am. Chem. Soc.*, 2018, **140**, 16042–16047.
102 B. Ma, G. Chen, C. Fave, L. Chen, R. Kuriki, K. Maeda, O. Ishitani, T.-C. Lau, J. Bonin and M. Robert, *J. Am. Chem. Soc.*, 2020, **142**, 6188–6195.
103 H. Kasap, D. S. Achilleos, A. Huang and E. Reisner, *J. Am. Chem. Soc.*, 2018, **140**, 11604–11607.
104 J. Ma, D. Jin, Y. Li, D. Xiao, G. Jiao, Q. Liu, Y. Guo, L. Xiao, X. Chen, X. Li, J. Zhou and R. Sun, *Appl. Catal., B*, 2021, **283**, 119520.
105 Y. Li, T. Kong and S. Shen, *Small*, 2019, **15**, 1900772.
106 A. Savateev, N. V. Tarakina, V. Strauss, T. Hussain, K. Brummelhuis, J. M. S. Vadillo, Y. Markushyna, S. Mazzanti, A. P. Tyutyunnik, R. Walczak, M. Oschatz, D. M. Guldi, A. Karton and M. Antonietti, *Angew. Chem., Int. Ed.*, 2020, **59**, 15061–15068.
107 S. N. Habisreutinger, L. Schmidt-Mende and J. K. Stolarczyk, *Angew. Chem., Int. Ed.*, 2013, **52**, 7372–7408.
108 X. Zhang, L. Yu, C. Zhuang, T. Peng, R. Li and X. Li, *ACS Catal.*, 2014, **4**, 162–170.
109 A. Kumar, P. Kumar, C. Joshi, S. Ponnada, A. K. Pathak, A. Ali, B. Sreedhar and S. L. Jain, *Green Chem.*, 2016, **18**, 2514–2521.
110 R. Kuriki, K. Sekizawa, O. Ishitani and K. Maeda, *Angew. Chem., Int. Ed.*, 2015, **54**, 2406–2409.
111 G. Zhao, H. Pang, G. Liu, P. Li, H. Liu, H. Zhang, L. Shi and J. Ye, *Appl. Catal., B*, 2017, **200**, 141–149.
112 W. Zhen and C. Xue, *Sol. RRL*, 2021, **5**, 2000440.
113 S. Xu, P. Zhou, Z. Zhang, C. Yang, B. Zhang, K. Deng, S. Bottle and H. Zhu, *J. Am. Chem. Soc.*, 2017, **139**, 14775–14782.
114 L. Dessbesell, S. Souzanchi, K. T. Venkateswara Rao, A. A. Carrillo, D. Bekker, K. A. Hall, K. M. Lawrence, C. L. J. Tait and C. Xu, *Biofuels, Bioprod. Biorefin.*, 2019, **13**, 1234–1245.
115 Y. Yang and T. Mu, *Green Chem.*, 2021, **23**, 4228–4254.
116 M. Sajid, X. Zhao and D. Liu, *Green Chem.*, 2018, **20**, 5427–5453.
117 Q. Zhang, X. Xiang, Y. Ge, C. Yang, B. Zhang and K. Deng, *J. Catal.*, 2020, **388**, 11–19.
118 P. Qi, S. Chen, J. Chen, J. Zheng, X. Zheng and Y. Yuan, *ACS Catal.*, 2015, **5**, 2659–2670.
119 H. Zhang, N. Li, X. Pan, S. Wu and J. Xie, *Green Chem.*, 2016, **18**, 2308–2312.
120 E. I. García-López, F. R. Pomilla, E. Bloise, X.-f. Lü, G. Mele, L. Palmisano and G. Marcì, *Top. Catal.*, 2020, 1–14.
121 X. Liu, X. Wen and R. Hoffmann, *ACS Catal.*, 2018, **8**, 3365–3375.
122 M. X. Chen, M. Zhu, M. Zuo, S. Q. Chu, J. Zhang, Y. Wu, H. W. Liang and X. Feng, *Angew. Chem.*, 2020, **59**, 1627–1633.
123 X.-H. Li and M. Antonietti, *Chem. Soc. Rev.*, 2013, **42**, 6593–6604.
124 P. Zhang, T. Song, T. Wang and H. Zeng, *Appl. Catal., B*, 2017, **206**, 328–335.
125 Y.-C. Chen, Y.-S. Huang, H. Huang, P.-J. Su, T.-P. Perng and L.-J. Chen, *Nano Energy*, 2020, **67**, 104225.
126 Q. Ding, Y. Shi, M. Chen, H. Li, X. Yang, Y. Qu, W. Liang and M. Sun, *Sci. Rep.*, 2016, **6**, 1–10.
127 A. P. Manuel, A. Kirkey, N. Mahdi and K. Shankar, *J. Mater. Chem. C*, 2019, **7**, 1821–1853.
128 S. Dong, M. Chen, J. Zhang, J. Chen and Y. Xu, *Green Energy Environ.*, 2020, DOI: 10.1016/j.gee.2020.07.004.
129 Y. Guo and J. Chen, *RSC Adv.*, 2016, **6**, 101968–101973.
130 J. Low, J. Yu, M. Jaroniec, S. Wageh and A. A. Al-Ghamdi, *Adv. Mater.*, 2017, **29**, 1601694.
131 J. Fu, J. Yu, C. Jiang and B. Cheng, *Adv. Energy Mater.*, 2018, **8**, 1701503.
132 Q. Xu, L. Zhang, B. Cheng, J. Fan and J. Yu, *Chem*, 2020, **6**, 1543–1559.

133 P. Zhou, J. Yu and M. Jaroniec, *Adv. Mater.*, 2014, **26**, 4920–4935.
134 Y. Wang, Q. Wang, X. Zhan, F. Wang, M. Safdar and J. He, *Nanoscale*, 2013, **5**, 8326–8339.
135 H. Li, Y. Zhou, W. Tu, J. Ye and Z. Zou, *Adv. Funct. Mater.*, 2015, **25**, 998–1013.
136 H. Zhang, Z. Feng, Y. Zhu, Y. Wu and T. Wu, *J. Photochem. Photobiol., A*, 2019, **371**, 1–9.
137 X. Xu, J. Zhang, S. Wang, Z. Yao, H. Wu, L. Shi, Y. Yin, S. Wang and H. Sun, *J. Colloid Interface Sci.*, 2019, **555**, 22–30.
138 Y. Zhu, Y. Zhang, L. Cheng, M. Ismael, Z. Feng and Y. Wu, *Adv. Powder Technol.*, 2020, **31**, 1148–1159.
139 T. Uekert, M. A. Bajada, T. Schubert, C. M. Pichler and E. Reisner, *ChemSusChem*, 2020, DOI: 10.1002/cssc.202002580.
140 X.-X. Wang, S. Meng, S. Zhang, X. Zheng and S. Chen, *Catal. Commun.*, 2020, **147**, 106152.
141 G. Gao, Q. Xi, H. Zhou, Y. Zhao, C. Wu, L. Wang, P. Guo and J. Xu, *Nanoscale*, 2017, **9**, 12032–12038.
142 S. Pradhan, D. Bhujel, B. Gurung, D. Sharma, S. Basel, S. Rasaily, S. Thapa, S. Borthakur, W. L. Ling and L. Saikia, *Nanoscale Adv.*, 2021, **3**, 1464–1472.
143 Y.-F. Xu, M.-Z. Yang, B.-X. Chen, X.-D. Wang, H.-Y. Chen, D.-B. Kuang and C.-Y. Su, *J. Am. Chem. Soc.*, 2017, **139**, 5660–5663.
144 J.-F. Liao, Y.-F. Xu, X.-D. Wang, H.-Y. Chen and D.-B. Kuang, *ACS Appl. Mater. Interfaces*, 2018, **10**, 42301–42309.
145 S. You, S. Guo, X. Zhao, M. Sun, C. Sun, Z. Su and X. Wang, *Dalton Trans.*, 2019, **48**, 14115–14121.
146 A. Speltini, L. Romani, D. Dondi, L. Malavasi and A. Profumo, *Catalysts*, 2020, **10**, 1259.
147 J. Yi, W. El-Alami, Y. Song, H. Li, P. M. Ajayan and H. Xu, *Chem. Eng. J.*, 2020, **382**, 122812.
148 S. Liu, F. Chen, S. Li, X. Peng and Y. Xiong, *Appl. Catal., B*, 2017, **211**, 1–10.
149 K. S. Lakhi, D.-H. Park, K. Al-Bahily, W. Cha, B. Viswanathan, J.-H. Choy and A. Vinu, *Chem. Soc. Rev.*, 2017, **46**, 72–101.
150 T. Chhabra, A. Bahuguna, S. S. Dhankhar, C. Nagaraja and V. Krishnan, *Green Chem.*, 2019, **21**, 6012–6026.
151 R. N. Baig, S. Verma, M. N. Nadagouda and R. S. Varma, *Sci. Rep.*, 2016, **6**, 1–6.
152 S. Verma, R. N. Baig, M. N. Nadagouda, C. Len and R. S. Varma, *Green Chem.*, 2017, **19**, 164–168.
153 P. Zhang, D. Sun, A. Cho, S. Weon, S. Lee, J. Lee, J. W. Han, D.-P. Kim and W. Choi, *Nat. Commun.*, 2019, **10**, 1–14.
154 Q. Liu, F. Wang, Y. Jiang, W. Chen, R. Zou, J. Ma, L. Zhong and X. Peng, *Carbon*, 2020, **170**, 199–212.
155 M. Ilkaeva, I. Krivtsov, E. I. García-López, G. Marcì, O. Khainakova, J. R. García, L. Palmisano, E. Díaz and S. Ordóñez, *J. Catal.*, 2018, **359**, 212–222.
156 L. Jiang, X. Yuan, Y. Pan, J. Liang, G. Zeng, Z. Wu and H. Wang, *Appl. Catal., B*, 2017, **217**, 388–406.
157 M. Zhang, X. Bai, D. Liu, J. Wang and Y. Zhu, *Appl. Catal., B*, 2015, **164**, 77–81.
158 S. Hu, X. Chen, Q. Li, F. Li, Z. Fan, H. Wang, Y. Wang, B. Zheng and G. Wu, *Appl. Catal., B*, 2017, **201**, 58–69.
159 X. Sun, D. Jiang, L. Zhang and W. Wang, *Appl. Catal., B*, 2018, **220**, 553–560.
160 J. Li, J. j. Zhang, H. y. Liu, J. l. Liu, G. y. Xu, J. x. Liu, H. Sun and Y. Fu, *ChemistrySelect*, 2017, **2**, 11062–11070.
161 L. Zhang, Y. Ren, W. Liu, A. Wang and T. Zhang, *Natl. Sci. Rev.*, 2018, **5**, 653–672.
162 S. K. Kaiser, Z. Chen, D. F. Akl, S. Mitchell and J. Pérez-Ramírez, *Chem. Rev.*, 2020, **120**, 11703–11809.
163 D. Liu, Q. He, S. Ding and L. Song, *Adv. Energy Mater.*, 2020, **10**, 2001482.
164 R. Lang, X. Du, Y. Huang, X. Jiang, Q. Zhang, Y. Guo, K. Liu, B. Qiao, A. Wang and T. Zhang, *Chem. Rev.*, 2020, **120**, 11986–12043.
165 P. Sharma, S. Kumar, O. Tomanec, M. Petr, J. Z. Chen, J. T. Miller, R. S. Varma, M. B. Gawande and R. Zbořil, *Small*, 2021, **17**, 2006478.
166 J. Fu, J. Lym, W. Zheng, K. Alexopoulos, A. V. Mironenko, N. Li, J. A. Boscoboinik, D. Su, R. T. Weber and D. G. Vlachos, *Nat. Catal.*, 2020, **3**, 446–453.
167 M. B. Gawande, P. Fornasiero and R. Zbořil, *ACS Catal.*, 2020, **10**, 2231–2259.
168 J. Wu, L. Xiong, B. Zhao, M. Liu and L. Huang, *Small Methods*, 2020, **4**, 1900540.
169 S. Tian, Z. Wang, W. Gong, W. Chen, Q. Feng, Q. Xu, C. Chen, C. Chen, Q. Peng and L. Gu, *J. Am. Chem. Soc.*, 2018, **140**, 11161–11164.
170 L. Wang, R. Tang, A. Kheradmand, Y. Jiang, H. Wang, W. Yang, Z. Chen, X. Zhong, S. P. Ringer and X. Liao, *Appl. Catal., B*, 2021, **284**, 119759.
171 I. F. Teixeira, E. C. Barbosa, S. C. E. Tsang and P. H. Camargo, *Chem. Soc. Rev.*, 2018, **47**, 7783–7817.
172 S. N. Talapaneni, G. Singh, I. Y. Kim, K. AlBahily, A. a. H. Al-Muhtaseb, A. S. Karakoti, E. Tavakkoli and A. Vinu, *Adv. Mater.*, 2020, **32**, 1904635.
173 Z.-F. Huang, J. Song, L. Pan, Z. Wang, X. Zhang, J.-J. Zou, W. Mi, X. Zhang and L. Wang, *Nano Energy*, 2015, **12**, 646–656.
174 J. Ran, T. Y. Ma, G. Gao, X.-W. Du and S. Z. Qiao, *Energy Environ. Sci.*, 2015, **8**, 3708–3717.
175 Z. Wang, M. Chen, Y. Huang, X. Shi, Y. Zhang, T. Huang, J. Cao, W. Ho and S. C. Lee, *Appl. Catal., B*, 2018, **239**, 352–361.
176 Y. Zhang, T. Mori, J. Ye and M. Antonietti, *J. Am. Chem. Soc.*, 2010, **132**, 6294–6295.
177 J. Fang, H. Fan, M. Li and C. Long, *J. Mater. Chem. A*, 2015, **3**, 13819–13826.
178 J. Ran, T. Y. Ma, G. Gao, X.-W. Du and S. Z. Qiao, *Energy Environ. Sci.*, 2015, **8**, 3708–3717.
179 X.-X. Fang, L.-B. Ma, K. Liang, S.-J. Zhao, Y.-F. Jiang, C. Ling, T. Zhao, T.-Y. Cheang and A.-W. Xu, *J. Mater. Chem. A*, 2019, **7**, 11506–11512.

180 S. Kumar, M. B. Gawande, J. Kopp, S. Kment, R. S. Varma and R. Zboril, *ChemSusChem*, 2020, **13**, 5231–5238.
181 J. Ma, D. Jin, X. Yang, S. Sun, J. Zhou and R. Sun, *Green Chem.*, 2021, **23**, 4150–4160.
182 X.-H. Li, X. Wang and M. Antonietti, *Chem. Sci.*, 2012, **3**, 2170–2174.
183 S. Yang, Y. Gong, J. Zhang, L. Zhan, L. Ma, Z. Fang, R. Vajtai, X. Wang and P. M. Ajayan, *Adv. Mater.*, 2013, **25**, 2452–2456.
184 C. Zhou, C. Lai, D. Huang, G. Zeng, C. Zhang, M. Cheng, L. Hu, J. Wan, W. Xiong and M. Wen, *Appl. Catal., B*, 2018, **220**, 202–210.
185 J. Zhang, F. Guo and X. Wang, *Adv. Funct. Mater.*, 2013, **23**, 3008–3014.
186 L. Luo, J. Ma, H. Zhu and J. Tang, *Nanoscale*, 2020, **12**, 7339–7346.
187 A. Vinu, K. Ariga, T. Mori, T. Nakanishi, S. Hishita, D. Golberg and Y. Bando, *Adv. Mater.*, 2005, **17**, 1648–1652.
188 H. Liu, H. Li, J. Lu, S. Zeng, M. Wang, N. Luo, S. Xu and F. Wang, *ACS Catal.*, 2018, **8**, 4761–4771.
189 V. R. Battula, A. Jaryal and K. Kailasam, *J. Mater. Chem. A*, 2019, **7**, 5643–5649.
190 R. Zhu, G. Zhou, J.-n. Teng, W. Liang, X. Li and Y. Fu, *Green Chem.*, 2021, **23**, 1758–1765.
191 H. Yan, *Chem. Commun.*, 2012, **48**, 3430–3432.
192 Z. Yang, Y. Zhang and Z. Schnepp, *J. Mater. Chem. A*, 2015, **3**, 14081–14092.
193 Q. Wu, Y. He, H. Zhang, Z. Feng, Y. Wu and T. Wu, *Mol. Catal.*, 2017, **436**, 10–18.
194 I. Krivtsov, E. I. García-López, G. Marcì, L. Palmisano, Z. Amghouz, J. R. García, S. Ordóñez and E. Díaz, *Appl. Catal., B*, 2017, **204**, 430–439.
195 A. Akhundi, E. I. García-López, G. Marcì, A. Habibi-Yangjeh and L. Palmisano, *Res. Chem. Intermed.*, 2017, **43**, 5153–5168.
196 A. Speltini, A. Scalabrini, F. Maraschi, M. Sturini, A. Pisanu, L. Malavasi and A. Profumo, *Int. J. Hydrogen Energy*, 2018, **43**, 14925–14933.
197 C. M. Pichler, T. Uekert and E. Reisner, *Chem. Commun.*, 2020, **56**, 5743–5746.
198 S. Das, D. Pandey, J. Thomas and T. Roy, *Adv. Mater.*, 2019, **31**, 1802722.
199 A. Li, W. Zhu, C. Li, T. Wang and J. Gong, *Chem. Soc. Rev.*, 2019, **48**, 1874–1907.